Evidence for microbial mediation of subseafloor nitrogen redox processes at Loihi Seamount, Hawaii

Jason B. Sylvan [a,*], Scott D. Wankel [b], Douglas E. LaRowe [c],
Chawalit N. Charoenpong [b,d], Julie A. Huber [e], Craig L. Moyer [f],
Katrina J. Edwards [a,c,1]

[a] *Department of Biological Sciences, University of Southern California, Los Angeles, CA 90089, United States*
[b] *Department of Marine Chemistry and Geochemistry, Woods Hole Oceanographic Institution, Woods Hole, MA 02543, United States*
[c] *Department of Earth Sciences, University of Southern California, Los Angeles, CA 90089, United States*
[d] *Department of Earth, Atmospheric and Planetary Sciences, Massachusetts Institute of Technology, Cambridge, MA 02139, United States*
[e] *Josephine Bay Paul Center, Marine Biological Laboratory, Woods Hole, MA 02543, United States*
[f] *Biology Department, Western Washington University, Bellingham, WA 98225, United States*

Abstract

The role of nitrogen cycling in submarine hydrothermal systems is far less studied than that of other biologically reactive elements such as sulfur and iron. In order to address this knowledge gap, we investigated nitrogen redox processes at Loihi Seamount, Hawaii, using a combination of biogeochemical and isotopic measurements, bioenergetic calculations and analysis of the prokaryotic community composition in venting fluids sampled during four cruises in 2006, 2008, 2009 and 2013. Concentrations of NH_4^+ were positively correlated to dissolved Si and negatively correlated to $NO_3^- + NO_2^-$, while NO_2^- was not correlated to $NO_3^- + NO_2^-$, dissolved Si or NH_4^+. This is indicative of hydrothermal input of NH_4^+ and biological mediation influencing NO_2^- concentrations. The stable isotope ratios of NO_3^- ($\delta^{15}N$ and $\delta^{18}O$) was elevated with respect to background seawater, with $\delta^{18}O$ values exhibiting larger changes than corresponding $\delta^{15}N$ values, reflecting the occurrence of both production and reduction of NO_3^- by an active microbial community. $\delta^{15}N$-NH_4^+ values ranged from 0‰ to +16.7‰, suggesting fractionation during consumption and potentially N-fixation as well. Bioenergetic calculations reveal that several catabolic strategies involving the reduction of NO_3^- and NO_2^- coupled to sulfide and iron oxidation could provide energy to microbes in Loihi fluids, while 16S rRNA gene sequencing of Archaea and Bacteria in the fluids reveals groups known to participate in denitrification and N-fixation. Taken together, our data support the hypothesis that microbes are mediating N-based redox processes in venting hydrothermal fluids at Loihi Seamount.
© 2016 Elsevier Ltd. All rights reserved.

Keywords: Hydrothermal vent; Nitrogen; Biogeochemistry; Isotopes; Bionergetics; Subsurface biosphere; Geomicrobiology; Loihi

1. INTRODUCTION

Loihi is a model system for mid-plate hotspot magmatism. Hydrothermal activity at Loihi seamount is dominated by low-temperature vents emitting fluids up to ~70 °C with elevated concentrations of dissolved Fe(II), CO_2, CH_4 and NH_4^+ (Gamo et al., 1987; Karl et al., 1989; Sedwick et al., 1992). In contrast to mid-ocean ridge

* Corresponding author at: Department of Oceanography, Texas A&M University, College Station, TX 77845, United States.
E-mail address: jasonsylvan@tamu.edu (J.B. Sylvan).
[1] Deceased 26 October 2014.

hydrothermal vents, hydrothermal fluids at Loihi are depleted in H_2S, making Loihi an excellent location to study microbial Fe-cycling (Emerson and Moyer, 2002; Glazer and Rouxel, 2009; Edwards et al., 2011).

Hydrothermal activity at Loihi is characterized by two modes of venting. At the summit, hydrothermal activity is currently present mostly in the Pele's Pit crater, which is home to the Hiolo North area of venting around 1300 meters (m) below sea level, the Pohaku area around 1178 m depth and the Hiolo South area around 1274 m (Karl et al., 1989; Sedwick et al., 1992; Glazer and Rouxel, 2009; Jesser et al., 2015). These three areas are characterized by diffuse flow venting of warm hydrothermal fluids ~20–50 °C with iron-rich microbial mats found near the vent sites. The microbial mats at Loihi's summit are generally dominated by members of the Zetaproteobacteria at sites with venting temperatures <40 °C, while increasing proportions of Epsilonproteobacteria are detected at sites with venting temperatures warmer than that (Moyer et al., 1994, 1995, 1998; Emerson and Moyer, 2002; Rassa et al., 2009).

Recently, a new type of hydrothermal activity was detected at the base of Loihi Seamount, at the site referred to as Ula Nui, located 5000 m deep at the base of the volcano. Venting at Ula Nui is characterized by ultra-diffuse venting, with a temperature anomaly only 0.2 °C above the ambient temperature of 1.7 °C (Edwards et al., 2011). This low temperature venting supports massive microbial mats that grow to >1 m tall and are largely dominated by Zetaproteobacteria.

In comparison to studies of sulfur redox processes in marine hydrothermal systems, there are far fewer studies of nitrogen redox processes. Recently, however, several studies have shown that genes involved in microbial nitrogen redox reactions are abundant in hydrothermal settings, including the presence of anaerobic ammonia oxidation (anammox) across a variety of hydrothermal settings (Byrne et al., 2009), nitrogen fixation genes (Mehta et al., 2003) and the presence of genes indicating multiple nitrogen redox pathways (Wang et al., 2009). In addition, the importance of denitrification in marine hydrothermal vent environments has become increasingly apparent (Wang et al., 2009; Xie et al., 2010; Bourbonnais et al., 2012a,b; Pérez-Rodríguez et al., 2013a; Bourbonnais et al., 2014; Vetriani et al., 2014). At Loihi, microbial mats that form adjacent to venting sites were consistently found to contain the copper containing nitrite reductase gene (nirK), which is indicative of the ability to perform denitrification (Jesser et al., 2015). The ubiquity of nitrogen redox transformations and the microbial communities catalyzing them, however, remains poorly understood in marine hydrothermal settings.

Following initial sampling and chemical characterization of end-member hydrothermal fluids at Loihi in the late 1980's, which revealed elevated NH_4^+ concentrations of 0.28–5.56 μM and an inverse relationship between NH_4^+ and $NO_3^- + NO_2^-$ (Karl et al., 1989; Sedwick et al., 1992), there have been no studies focusing on nitrogen (N) cycling. Here, we investigate nitrogen cycling processes at Loihi Seamount using a combination of biogeochemical and iso-topic measurements, bioenergetic calculations and analysis of the prokaryotic community composition. While the microbial mats at Loihi have been well characterized (Moyer et al., 1994, 1995, 1998; Emerson and Moyer, 2002; Rassa et al., 2009; Edwards et al., 2011; Jesser et al., 2015), the microbiology of the venting fluids has not been previously described. Our analysis reveals the occurrence of several nitrogen redox transformations in Loihi subsurface fluids and sheds light on the putative microbial lineages associated with them.

2. SAMPLING AND ANALYTICAL METHODS

2.1. Sampling

Four cruises were conducted to Loihi Seamount: 22 September–10 October 2008 and 16 March–01 April 2013 aboard *R/V Thomas G. Thompson* and 11–27 October 2006 and 01–17 October 2009 aboard *R/V Kilo Moana*. We sampled hydrothermal fluid samples, labeled "Vent Fluids" in Table 1, from sites at Hiolo North (M31, M36, M39), Hiolo South (M34 and M38; previously named Loihau, renamed Hiolo South by Jesser et al., 2015;), Pohaku (M57), Pit of Death (M56) and Ula Nui. Areas and sites sampled are labeled in Fig. 1. Background seawater samples were collected away from venting in Pele's Pit, Pit of Death, and at Ula Nui (Table 1). Non-buoyant hydrothermal plume samples, labeled "Water Column Profiles" in Table 1, were collected in Pele's Pit and Pit of Death and during a Tow-Yo CTD cast southwest of Loihi's summit (Bennett et al., 2011). In addition to these sites, which have been visited in previous studies of Loihi (Glazer and Rouxel, 2009; Edwards et al., 2011; Jesser et al., 2015), two new sites were discovered and sampled in the Hiolo South area (near Markers 34 and 38) during the 2009 expedition (Table 1). One new area of venting chimlets (small iron-oxide chimneys) was discovered between Markers 34 and 38 (labeled M34 → M38). The other new site was an approximately meter tall Fe-oxyhydroxide chimney dubbed "Red Smoker".

Hydrothermal vent samples destined for chemical analysis were collected from venting fissures in basalt rocks, ferruginous chimneys and a microbial mat (sample 477-MS-blue) using a titanium Major sampler deployed from *ROV Jason II*. The operation of the Major samplers for hydrothermal vent research has been described previously (Von Damm et al., 1985), as well as specifically for Loihi (Glazer and Rouxel, 2009). The Major sampler was placed directly in the venting orifice for rocky fissures and into the mouth of ferruginous chimneys. The ferruginous chimney structures are very delicate, therefore care was taken to place the snorkel of the Major sampler inside of the chimneys without causing the structure to collapse. For the mat sample collected with a Major sampler at Ula Nui, the sampling snorkel was pressed approximately 15 cm below the surface of the 1 m tall mat and triggered.

During the 2013 cruise, a newly designed microbial mat sampler (Breier et al., 2012) was used to specifically sample depth profiles within microbial mats. Briefly, the samplers consist of six 60-ml syringes arranged on a cassette for

Table 1
Composition of hydrothermal vent fluids, microbial mat samples ("-BM1-"), background seawater, and water column profiles collected from Loihi Seamount during 2008 (sample name begins with 3xx or 08xx-xx), 2009 (sample name begins with 4xx or 09xx-xx) and 2013 (sample name begins with 6xx). Units of measurement for biogeochemical measurements are µM, depth is in meters, bd = below detection, – = not measured.

Site	Sample	Depth	Temp (°C)	NH_4^+	NO_2^-	$NO_3^- + NO_2^-$	dSi	PO_4^{3-}
Vent fluids								
Hiolo North area								
M36	476-MS-blue	1303	35.6	2.615	–	0.82	–	3.00
M39	479-MS-black	1300	45.8	2.074	–	14.09	–	2.00
M39	482-MS-blue	1301	42.7	2.724	–	8.17	–	3.00
M39	482-MS-red	1301	42.7	2.291	–	3.19	–	3.20
M31	482-MS-black	1297	40.6	2.357	–	1.52	–	3.20
M31	476-MS-red	1301	43	2.815	–	1.27	–	
M31	675-MS-black2	1300	41.3	2.278	0.095	1.55	500.6	4.44
M31	672-MS-yellow	1300	40.7	2.096	0.093	1.86	218.6	3.70
M31	675-MS-red2	1300	41.3	2.122	0.142	1.51	464.6	3.82
M39	674-MS-black	1302	25.7	1.122	0.259	16.34	268.6	0.69
Upper M31	674-MS-yellow	1300	–	1.584	0.493	6.86	310.6	1.06
47 deg site	672-MS-black	1298	47.1	2.721	bd	1.05	270.6	2.35
Directly above M31, near M39, ~25 cm above orifice	676-MS-white	1300	–	1.322	bd	22.30	286.6	0.26
Directly above M31, near M39, same site as 676-MS-white, in orifice	676-MS-yellow	1300	41.2	2.096	bd	4.02	456.6	3.76
Texture Garden (between M31 & M39)	676-MS-black	1298	30.8	3.032	0.236	11.82	352.6	2.72
Hiolo South area								
M38	675-MS-white	1274	43.3	2.408	bd	2.91	432.6	6.64
M38	675-MS-yellow	1274	42.4	2.647	bd	2.67	522.6	6.40
M34	675-MS-black	1272	47.4	1.925	0.215	4.53	700.6	6.22
M34	675-MS-yellow2	1270	48.2	2.660	bd	1.38	488.6	3.82
M34	675-MS-red	1272	47.4	0.705	bd	25.21	256.6	3.33
M34	675-MS-white2	1270	48.1	2.508	bd	1.164	450.6	6.09
M34	479-MS-blue	1273	50.1	4.249	–	7.22	–	4.50
M34	483-MS-white	1273	50.7	2.398	–	24.39	–	2.90
M34	476-MS-black	1272	41.8	3.655	–	1.37	–	–
M34	373-MS-red	1271	51.5	7.506	–	–	–	2.39
M34	373-MS-black	1271	51.5	3.606	–	–	–	1.26
M34, few cm into mat	675-BM1-C2	1271	–	2.128	0.166	31.73	426.6	1.12
M34, few cm into mat	675-BM1-C4	1271	–	2.536	0.149	22.68	448.6	1.47
M34, ~1–2 cm into diffuse flow orifice with mat surrounding orifice, same area as C4	675-BM1-C6	1271	–	3.088	0.347	26.37	432.6	2.73
M34->M38	483-MS-black	1276	47.4	0.754	–	30.82	–	0.90
M38	479-MS-white	1274	42	3.114	–	8.87	–	3.00
Red Smoker	483-MS-blue	1254	47.4	2.951	–	13.17	–	2.90
Pohaku area								
M57	368-MS-red	1178	26.7	4.090	–	9.03	689.6	2.31
M57	368-MS-black	1178	28.3	2.808	–	20.70	605.6	0.73
M57	476 MS-white	1178	24	2.431	–	21.13	–	
M57	671-MS-white	1177	25.9	4.211	0.333	17.70	160.6	3.21
M57	671-MS-red	1177	25.9	4.235	0.124	30.01	210.6	0.45
Ula Nui area								
Ula Nui Mat	477-MS-blue	4984	2.8	1.555	–	25.27	–	4.10
Ula Nui 'orange mat 1' surface	673-BM1-A2	4983	–	0.608	0.185	21.67	303	3.07
Ula Nui 'black mat 1' surface	673-BM1-A3	4983	–	0.511	bd	30.25	231	2.92

Table 1 (*continued*)

Site	Sample	Depth	Temp (°C)	NH_4^+	NO_2^-	$NO_3^- + NO_2^-$	dSi	PO_4^{3-}
Ula Nui 'orange mat 2' surface	673-BM1-C5	4988	–	0.515	bd	31.95	183	2.43
5 cm in mat C5	673-BM1-B2	4988	–	1.845	0.280	5.91	447	3.12
15 cm in mat C5	673-BM1-B4	4988	–	2.094	0.178	3.28	451	2.70
Ula Nui 'black mat 2' surface	673-BM1-D6	4988	1.8	0.554	bd	35.35	139	2.28
5 cm in mat D6	673-BM1-D4	4988	1.8	1.197	bd	18.68	301	0.89
15 cm in of mat D6	673-BM1-D2	4988	1.8	2.131	bd	5.71	435	0.55
Pit of death								
M56	365-MS-black	1199	4.5	0.201	–	36.67	–	1.36
Background seawater								
M31 SW	482-port-niskin	1297	3.8	1.130	–	43.19	–	2.76
M31 SW	482-strbrd-niskin	1297	3.8	0.617	–	36.77	–	2.65
M57 SW	476-niskin	1179	5	0.015	–	42.61	–	2.84
M57 SW	676-BM2-D6	1185	4	0.073	bd	40.12	126.6	1.43
M57 Elevator	676-MS-red	1311	4	0.440	bd	41.04	108.6	2.35
Ula Nui SW	477-niskin	4984	2.6	0.560	–	36.31	–	2.57
M56 SW	365-niskin	1297	3.9	0.201	–	40.60	–	3.07
Water column profiles								
Pele's Pit CTD casts								
Pele's Pit, 2008	0801-21	900	4.7	bd	–	38.10	79.6	3.00
Pele's Pit, 2009	0901-21	801	4.9	bd	–	42.81	86.8	3.37
Pele's Pit, 2009	0901-16	1051	4.0	1.200	–	36.45	74.8	3.35
Pele's Pit, 2009	0901-14	1150	3.7	0.690	–	42.76	116.8	3.26
Tow-yo west of summit								
SW of Loihi	0904-02	1139	3.7	0.286	–	41.79	108.8	2.69
SW of Loihi	0904-11	1207	3.6	0.324	–	28.44	85.8	2.80
SW of Loihi	0904-15	1166	3.7	0.167	–	41.41	95.8	3.40
SW of Loihi	0904-22	1177	3.4	0.213	–	41.60	120.8	3.35
Pit of death CTD cast								
Pit of death, 2009	0905-19	1076	3.9	0.076	–	47.22	101.8	3.24
Pit of death, 2009	0905-01	1286	3.7	1.500	–	45.28	105.8	3.37

which the syringe being sampled and speed of sampling is driven by a motor to allow for precise sampling of mats at specific depths. For samples destined for chemical analysis, a 0.2 μm syringe tip filter was placed inline so that the sample was filtered *in situ* as it was drawn into the syringe.

Background seawater samples were collected away from venting sites using Niskin bottles attached to the side of *ROV* Jason II. In one case, a Major sampler was fired away from venting to collect a background sample, and in another case, a single syringe of the mat sampler was used for background seawater. Water column profiles were conducted and hydrothermal plume samples were targeted and collected using niskin bottles on a CTD rosette. The plume emanating from Loihi's summit was detected using transmissometry, as detailed in Bennett et al. (2011).

All samples for chemical analysis were either filtered and then frozen (all samples from 2008 and 2013, CTD samples in 2009) or frozen immediately and filtered upon thawing before analysis (2009). For those filtered prior to freezing, samples from Major samplers were filtered through a 0.20 μm pore size syringe tip filter placed inline with the outlet of the Major sampler. Water column profile samples were filtered as they exited the niskin bottles with 0.20 μm pore size, 47 mm diameter Supor filters (Pall) in PFA filter holders (Cole-Parmer). All other samples were filtered using syringe tip filters on 60 ml syringes. Samples were stored in sterile polypropylene containers until analysis. An aliquot of sample was used to rinse the containers and discarded prior to filling the containers with sample.

Four diffuse flow hydrothermal fluid samples and two background seawater samples were sampled for microbial community analysis during the 2006 cruise (Table 2). LoihiPP1, 2, 4, 5 and 6 were sampled using the pelagic pump on the *ROV* Jason II during dives J2-241, J2-242, J2-243, J2-245 and J2-246, respectively. A hose with a course mesh filter at the sampling point was placed in venting diffuse fluids (LoihiPP1, 2, 5 and 6), and ~50 L was then filtered through a Steripak-GP 0.22 μm pore size filter. The filter was frozen at −80 °C upon retrieval of the vehicle. One background seawater sample (LoihiPP4) was collected in the same manner (~125 L filtered through a Steripak-GP) while the ROV was in the water column in Pele's Pit. Another background seawater sample, LoihiCTD03, was collected with a CTD rosette in Pele's Pit and then 10 L filtered through a Sterivex GP 0.22 μm pore size filter.
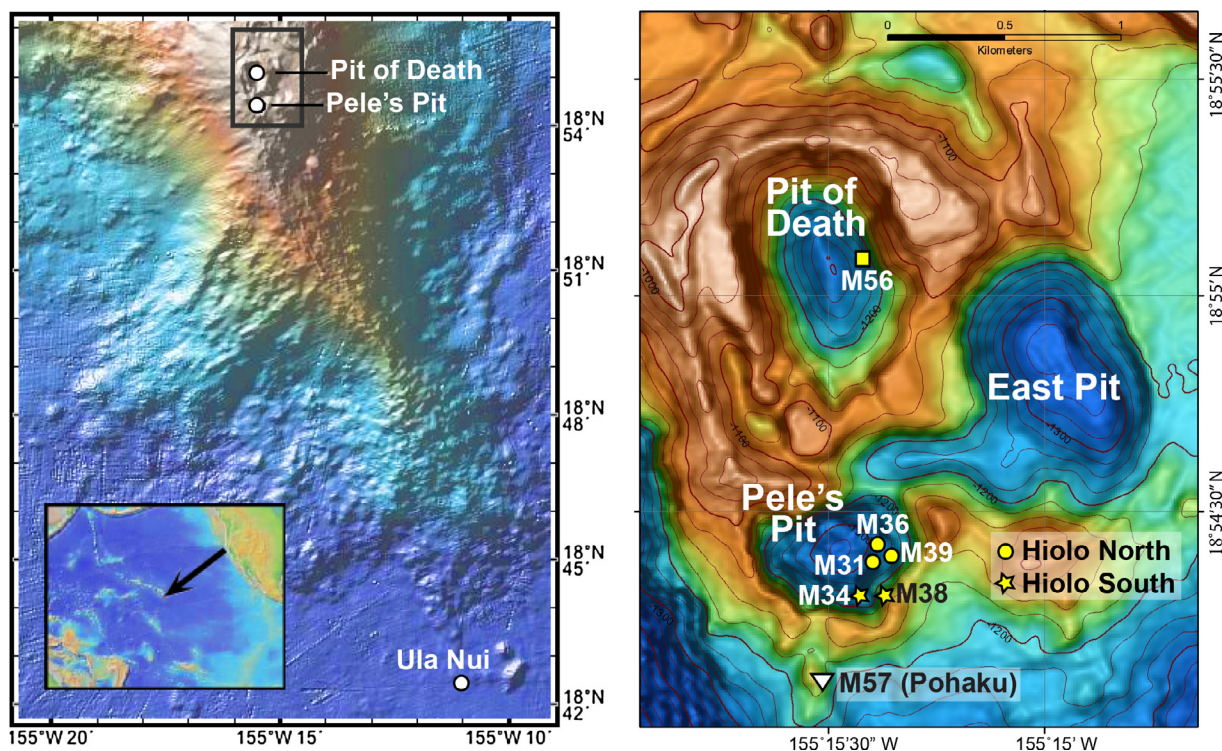
Fig. 1. Map of Loihi Seamount, with sampling sites indicated. Inset at the bottom of the left panel indicates the location of Loihi in the Pacific Ocean. Rectangle at the top of the left panel highlights the location of the area in the right panel. Sites marked by a yellow circle in the right panel are in Hiolo North and sites marked by a yellow star are in Hiolo South, as indicated by the key at right.

Table 2
Basic data for samples from which DNA sequences were obtained.

Sample	Date collected	Site	Depth (m)	# V6 Tags	#V6 tags after removing background OTUs
Vent fluids					
LoihiPP1-bac	27 Oct 2006	Marker 34	1272	11,707	1855
LoihiPP1-arc				21,806	3901
LoihiPP2-bac	31 Oct 2006	Hiolo North Area	1302	14,035	6947
LoihiPP2-arc				13,616	4540
LoihiPP5-bac	05 Nov 2006	Marker 31	1301	20,105	3812
LoihiPP5-arc				19,045	1969
LoihiPP6-bac	07 Nov 2006	Ula Nui	4987	16,200	1887
LoihiPP6-arc				13,961	336
Background seawater					
LoihiCTD03-bac	31 Oct 2006	Pele's Pit	1100	19,108	–
LoihiCTD03-arc				14,790	–
LoihiPP4-bac	02 Nov 2006	Pele's Pit	1717	18,682	–
LoihiPP4-arc				15,336	–

2.2. Chemistry analytical methods

Fluid temperatures were measured by placing the temperature probe on *ROV* Jason II into the venting orifice or chimney. $NO_3^- + NO_2^-$ (hereafter referred to as $NO_3 + NO_2$) and NO_2^- were measured using the chemiluminescent method after reduction to NO by hot, acidic vanadium ($NO_2 + NO_3$) or potassium iodide (NO_2^-) (Garside, 1982) with a detection limit of <0.010 μM. NH_4^+ was measured colorimetrically via the phenol-hypochlorite method

(Grasshoff et al., 1999) with a 5 cm cell in a Shimadzu UV-1601 spectrophotometer onboard the *R/V Thompson* (2008) or using the fluorescence method (Holmes et al., 1999) post-cruise (2009 and 2013). The detection limit for NH_4^+ by both methods is 0.030 μM. Spiked samples were within 5% of expected values or better for both methods. Dissolved inorganic phosphorus (P_i) and dissolved silica (dSi) were measured using colorimetric methods, with detection limits of 0.030 μM for P_i and 0.30 μM for dSi (Gieskes et al., 1991; Grasshoff et al., 1999).

To determine if vent fluid chemistry differed between Hiolo North, Hiolo South and Pohaku, one-way analysis of variance (ANOVA) was calculated with Tukey's posthoc pairwise comparison for hydrothermal vent fluid temperature and all chemical variables measured using JMP Pro 10 (SAS Institute, Inc.). Correlations between the same chemical variables across all samples were determined using Kendall's τ correlation.

2.3. Isotopic measurements

Nitrate N and O stable isotope ratios ($^{15}N/^{14}N$ and $^{18}O/^{16}O$, respectively) were measured using the denitrifier method (Sigman et al., 2001; Casciotti et al., 2002), in which sample NO_3^- is quantitatively converted to N_2O using a lab-grown denitrifying bacterium before being extracted and purified on a purge and trap system similar to that previously described in McIlvin and Casciotti (2010). Isotope ratios are expressed using standard delta notation where $\delta^{15}N = ((^{15}R_{sample}/^{15}R_{ref}) - 1) * 1000$ and ^{15}R refers to the $^{15}N/^{14}N$ ratio (or $^{18}O/^{16}O$ for $\delta^{18}O$). Nitrogen isotope ratios are reported relative to N_2 in air as reference, while oxygen isotope ratios are reported relative to Vienna Standard Mean Ocean Water (VSMOW). Where detected, NO_2^- was removed by sulfamic acid addition (Granger and Sigman, 2009) prior to isotopic analysis of NO_3^-. Isotope ratios were measured on an IsoPrime100 (Elementar, Inc.) and corrections for drift, size and fractionation of O isotopes during bacterial conversion were carried out as previously described using NO_3^- standards USGS 32, USGS 34 and USGS 35 (Casciotti et al., 2002; McIlvin and Casciotti, 2010), with a typical reproducibility of 0.2‰ and 0.4‰ for $\delta^{15}N$ and $\delta^{18}O$, respectively.

Analysis of ammonium nitrogen isotope ratios ($\delta^{15}N$-NH_4^+) was carried out by persulfate oxidation to NO_3^- as described previously (Knapp et al., 2005) followed by the denitrifier method to produce N_2O for purification and isotopic analysis. Samples were passed through a solid phase extraction (SPE) cartridge (Agilent Bond Elut PPL) to remove most of any dissolved organic nitrogen (Dittmar et al., 2008), as confirmed by the difference in the concentrations of total dissolved nitrogen taken after persulfate oxidation in the samples that passed and did not pass through the SPE cartridges. The resulting persulfate-converted sample provides $\delta^{15}N$ of (NO_3^- + NO_2^- + NH_4^+) while a parallel sample without persulfate oxidation step yields $\delta^{15}N$ of (NO_3^- + NO_2^-). Isotopic composition of the NH_4^+ pool was calculated by mass balance to report $\delta^{15}N$-NH_4^+ values, which were normalized to international isotopic reference standards: IAEA-N1 ($\delta^{15}N = 0.5‰$), USGS-25 ($\delta^{15}N = -29.4‰$) and USGS-26 ($\delta^{15}N = 52.9‰$).

2.4. Bioenergetic calculations

Values of the energy densities of the rth reaction per kg of water, E_r, are calculated using (LaRowe et al., 2014):

$$E_r = \left| \frac{\Delta G_r}{v_i} \right| [i] \qquad (1)$$

where v_i and $[i]$ stand for the stoichiometric coefficient and molal concentration, respectively, of the ith limiting electron donor or acceptor. Because either the electron donor or acceptor will be a limiting reactant per volume of fluid, the concentration and stoichiometric coefficient of this limiting nutrient were used for values of v_i and $[i]$ in Eq. (1). In order to carry out these calculations, the activities of all reactants and products were held constant. In effect, this is an instantaneous snapshot of the total amount of Gibbs energy contained in a kg of water for a particular reaction. Because the prevailing physiochemical conditions at the sample sites vary with time, Gibbs energy densities were calculated for high and low energy scenarios in order to capture the natural variability of hydrothermal vents at Loihi. The high energy scenario was generated using the highest concentrations of reactants and lowest concentrations of product species at each sample site. Conversely, the low energy scenario used the lowest concentrations of reactants and highest concentrations of product species at each sample site.

Values of ΔG_r are calculated using

$$\Delta G_r = -RT \ln \frac{K_r}{Q_r}, \qquad (2)$$

where K_r and Q_r refer to the equilibrium constant and reaction quotient of the reaction, respectively, R represents the gas constant, and T denotes temperature in Kelvin. Values of K_r were calculated using the revised-HKF equations of state (Helgeson et al., 1981; Tanger and Helgeson, 1988; Shock et al., 1992), the SUPCRT92 software package (Johnson et al., 1992), and thermodynamic data taken from a number of sources (Shock and Helgeson, 1988, 1990; Shock et al., 1989; Sverjensky et al., 1997; Schulte et al., 2001). Values of Q_r were calculated using

Table 3
Reactions considered in this study.

Iron oxidation with nitrate reduction
01. $2Fe^{2+} + NO_3^- + 3H_2O \rightarrow 2FeOOH + NO_2^- + 4H^+$
02. $5Fe^{2+} + NO_3^- + 7H_2O \rightarrow 5FeOOH + 0.5N_2 + 9H^+$
03. $8Fe^{2+} + NO_3^- + 13H_2O \rightarrow 8FeOOH + NH_4^+ + 14H^+$
04. $3Fe^{2+} + NO_2^- + 4H_2O \rightarrow 3FeOOH + 0.5N_2 + 10H^+$
05. $6Fe^{2+} + NO_2^- + 10H_2O \rightarrow 6FeOOH + NH_4^+ + 10H^+$

Methane oxidation with nitrate or nitrite reduction
06. $CH_4 + 4NO_3^- \rightarrow CO_2 + 4NO_2^- + 2H_2O$
07. $5CH_4 + 8NO_3^- + 8H^+ \rightarrow 5CO_2 + 4N_2 + 14H_2O$
08. $CH_4^+ + NO_3^- + 2H^+ \rightarrow CO_2 + NH_4^+ + H_2O$
09. $3CH_4 + 4NO_2^- + 8H^+ \rightarrow 3CO_2 + 4N_2 + 10H_2O$
10. $3CH_4 + 4NO_2^- + 8H^+ \rightarrow 3CO_2 + 4NH_4^+ + 2H_2O$

Sulfide oxidation with nitrate or nitrite reduction
11. $5H_2S + 8NO_3^- \rightarrow 5SO_4^{2-} + 4N_2 + 2H^+ + 4H_2O$
12. $H_2S + NO_3^- + H_2O \rightarrow SO_4^{2-} + NH_4^+$
13. $3H_2S + 8NO_2^- + 2H^+ \rightarrow 3SO_4^{2-} + 4N_2 + 4H_2O$
14. $3H_2S + 4NO_2^- + 4H_2O + 2H^+ \rightarrow 3SO_4^{2-} + 4NH_4^+$

Anammox
15. $NH_4^+ + NO_2^- \rightarrow N_2 + 2H_2O$

Ammonium or nitrite oxidation
16. $NH_4^+ + 1.5O_2 \rightarrow NO_2^- + H_2O + 2H^+$
17. $NO_2^- + 0.5O_2 \rightarrow NO_3^-$

Table 4

Temperatures and concentrations (μM) of select species used in the thermodynamic calculations at the indicated samples sites. The concentrations of species used in calculations but not measured here or specifically at the sites sampled here are as follows: CH_4 $(aq) = 177$ nM, average of values from (Karl et al., 1989); pH = 6.2 average of values taken from (Glazer and Rouxel, 2009); $SO_4^{2-} = 28$ mM (seawater); N_2 $(aq) = 0.51$ mM (equilibrium with $N_2(g)$ in atmosphere); CO_2 (aq) 18 mM (Karl et al., 1989); O_2 $(aq) = 4$ μM (this is a nominal microaerobic value).

Site	T, °C	NO_2^{-}[a]	NO_3^{-}[b]	NH_4^{+}[a]	Fe^{2+}	HS^-
Hiolo South	41.8–51.5[a]	0.144–0.347	1.16–31.70	0.754–7.506	346–6484[c]	11.6–25.2[c]
Pohaku	24.0–28.3[a]	0.124–0.333	9.03–41.04	2.430–4.235	507–773[c]	1.0[d]
Hiolo North	25.7–27.1[a]	0.093–0.493	0.82–22.30	1.320–3.030	117–799[c]	18.5[c]
Ula Nui						
Mat surface	2.0[e]	0–0.185	21.67–35.35	0.515–1.555	38–40[f]	1.0[d]
Mat 5 cm	2.0[e]	0–0.280	5.91–18.68	1.197–1.845	50–53[f]	1.0[d]
Mat 15	2.0[e]	0–0.178	3.28–5.71	2.094–2.131	85–86[f]	1.0[d]

[a] From values reported in Table 1.
[b] Calculated from $[NO_3^-] = [NO_3 + NO_2] - [NO_2^-]$ where values of $[NO_3 + NO_2] - [NO_2^-]$ are taken from Table 1.
[c] Glazer and Rouxel (2009).
[d] Nominal value.
[e] Assumed to be the same as bottom water.
[f] Edwards et al. (2011).

$$Q_r = \prod_i a_i^{v_i}, \quad (3)$$

where a_i stands for the activity of the ith species and v_i corresponds to the stoichiometric coefficient of the ith species in the reaction of interest. Values of a_i are related to the concentration of the ith species, C_i, through

$$a_i = \gamma_i \left(\frac{C_i}{C_i^\theta} \right) \quad (4)$$

where γ_i stands for the activity coefficient of the ith species and C_i^θ refers to the concentration of the ith species under standard state conditions, which is taken to be equal to one molal referenced to infinite dilution. Values of γ_i were in turn computed as a function of temperature and ionic strength using an extended version of the Debye-Hückel equation (Helgeson, 1969).

The reactions chosen to represent the catabolic potential of nitrogen-processing microbial communities at Loihi are comprised of electron donors (EDs) and electron acceptors (EAs) that are known to be present at this site (Table 3). Concentrations of NO_3^-, NO_2^-, NH_4^+ used in these calculations are reported in the current study, and the concentrations of other species, such as Fe^{2+} and HS^-, have been taken from other studies that have focused on the same sample sites (Glazer and Rouxel, 2009; Edwards et al., 2011); the data used is presented in Table 4.

2.5. DNA extraction, sequencing and data processing

Environmental DNA from diffuse flow fluids and background seawater was extracted using previously described methods (Sogin et al., 2006). Polymerase chain reaction of the V6 hypervariable region of the small subunit (SSU) rRNA gene for Bacteria and Archaea, followed by 454 pyrosequencing of the amplicons, was carried out as described previously for all diffuse flow and background seawater samples (Huber et al., 2007). Basic metadata for the samples used for pyrosequencing is given in Table 2.

Obtained sequences were run through the VAMPS pipeline (http://vamps.mbl.edu), which removed sequences with any N's and trimmed primers, requiring an absolute match to the sequencing primers. Phylogenetic affiliations of the tag sequences (hereafter referred to as pyrotags) were identified using the Global Alignment for Sequence Taxonomy (GAST) method (Huse et al., 2008) for all samples. For pyrotags designated "unknown" by GAST, each individual sequence was submitted to the RDP classifier with the bootstrap parameter set to 80% (Cole et al., 2009). If the sequence was not assigned to the domain Bacteria for sequences obtained using bacterial primers, or Archaea for sequences obtained using archaeal primers, it was removed from further analysis. Operational taxonomic units, defined at the 97% similarity cutoff, were determined using the software package Mothur (Schloss et al., 2009) with the pre.cluster command, which preclusters at a 1% difference level (one bp difference for the V6 tags used here) using modified single-linkage (Huse et al., 2010) and the average neighbor method. To concentrate on operational taxonomic units (OTUs) present only in diffuse fluids, we removed from our samples any OTUs (defined at the 97% similarity cutoff) that were present in the two Loihi seawater samples (LoihiCTD03 and LoihiPP4) using the remove.otus command in mothur.

Raw sequence data is deposited in the NCBI SRA under Bioproject PRJNA109379. Quality-controlled trimmed reads can be found at vamps.mbl.edu under projects KCK_SMT_Av6 and KCK_SMT_Bv6.

3. RESULTS

3.1. Bulk chemistry

Hydrothermal venting at Loihi is most active near the Pele's Pit crater. The mean temperature of the venting fluids in the Hiolo South area was ∼47 °C, ∼7 °C higher than the Hiolo North vents (Table 1). NH_4^+ concentrations were always elevated in comparison to background seawater

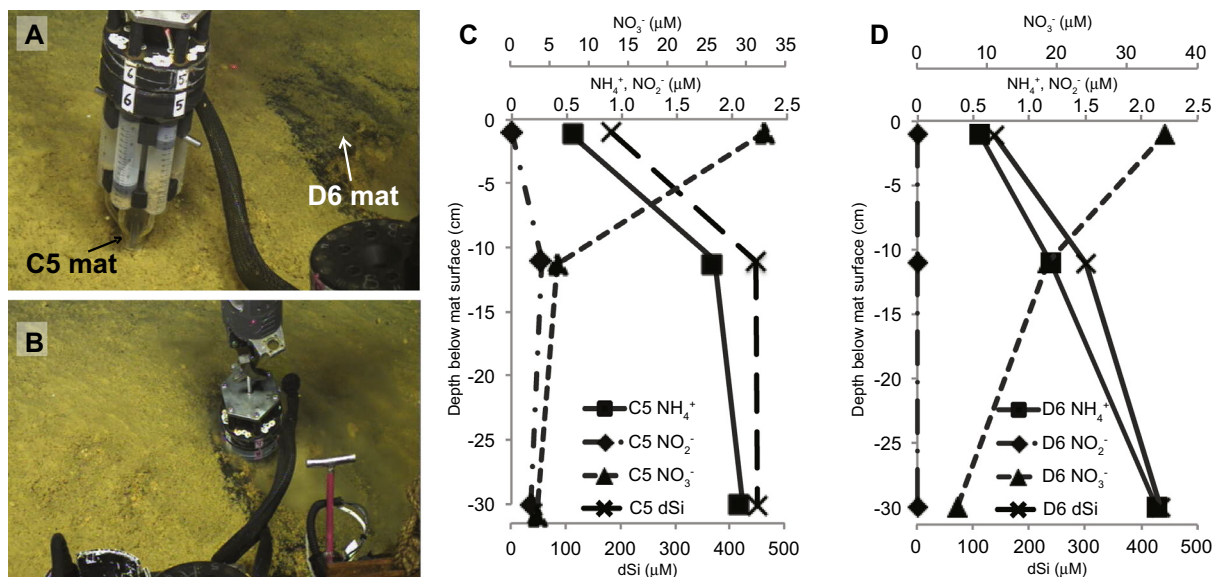Fig. 2. Depth profiles of dSi, NO_3, NO_2^- and NH_4^+ within two microbial mats at Ula Nui. (A) Mat sampler collecting fluids from the surface of mat C5. Mat D6 can be seen to the left of the photograph. (B) Mat sampler collecting fluids at a depth of 15 cm in mat C5. (C) Depth profile in mat C5. (D) Depth profile in mat D6.

(<0.03 µM), ranging from 1.1 µM to 3.0 µM in the Hiolo North area, ~0.7 µM lower, on average, than those measured in the Hiolo South area (range 0.7–7.5 µM). Pohaku/M57, located on the outside rim of Pele's Pit (Fig. 1), emits end-member fluids with a mean temperature of 26 °C and NH_4^+ concentrations from 2.4 to 4.2 µM. The diffuse venting and background seawater samples in the Pit of Death contained elevated NH_4^+ (0.2 µM) compared to typical deep ocean waters (<0.03 µM, samples 0801-21 and 0901-21, Table 1) in 2008, but this site was found to be inactive in 2009 and not sampled again. $NO_3 + NO_2$ concentrations ranged widely at both Hiolo North and the Hiolo South area, but were higher, on average, in the Hiolo South area, and all samples were generally much lower than background seawater (~41 µM). NO_2^- ranged from below detection up to 0.5 µM at various sites in the Hiolo South, Hiolo North and Pohaku areas. P_i was variable, ranging from 0.3 µM, approximately an order of magnitude less than background seawater, to 6.6 µM, approximately twice background seawater.

Loihi seamount is home to abundant ferruginous microbial mats (Karl et al., 1988; Emerson and Moyer, 2002). Concentrations of Fe^{2+} and oxygen are known to be variable from the surface to the deeper parts of these mats; oxygen decreases from saturation to below detection by 10 cm below the mat surface and dissolved Fe^{2+} increases continuously from 40 µM at the surface of the mat to >120 µM at 70 cm below mat surface (Edwards et al., 2011). The interstitial space in these mats is comprised of a mix of background seawater and hydrothermal fluids from either the nearest orifice, as is the case with samples collected from the caldera, or from the bottom of the mat, as is the case with the mounds sampled at Ula Nui (Fig. 1). Samples obtained from a few cm below the surface of mats located at M34 all had elevated NH_4^+, NO_2^- and dSi compared to

background seawater concurrent with reduced concentrations $NO_3 + NO_2$ (Table 1). Sampling at the surface of four microbial mats at the ultra-diffuse venting Ula Nui site, known for meter tall nontronite laden mats (Edwards et al., 2011), revealed similar patterns. Additional information was gained from vertical profiling of two of these mats, which revealed increasing NH_4^+ and dSi and decreasing NO_3^- with depth (Fig. 2). Mat C5 also had increasing NO_2^- with depth while NO_2^- was below detection in mat D6, which was located only 20 cm away. The gradients in the top 5 cm were steeper in mat C5 than mat D6.

In hydrothermal vent fluids from Loihi, Mg remains close to background seawater, unlike high temperature hydrothermal venting (Karl et al., 1989; Sedwick et al., 1992; Glazer and Rouxel, 2009). Therefore, concentrations of dSi are used as a conservative tracer of Loihi hydrothermal vent fluids because they are elevated compared to background and mix conservatively with deep ocean water. NO_2^- does not show a relationship to dSi (Fig. 3C), while NH_4^+ is positively correlated to dSi (Fig. 3A). Two samples from M57 collected in 2013 had anomalously high dSi and are outliers to the trendline although believed to be accurate. $NO_3 + NO_2$ and NH_4^+ are negatively correlated (Fig. 3B), as has been noted before (Karl et al., 1989; Sedwick et al., 1992). The linear relationships between both NH_4^+ vs dSi and $NO_3 + NO_2$ vs NH_4^+ are variable dependent on the year of sampling, including data from previous studies (Karl et al., 1989; Sedwick et al., 1992) (Fig. 3A and B).

One-way ANOVA was used to statistically compare the end-member fluid data (Table 5) from Hiolo North, Hiolo South and Pohaku. Hydrothermal fluid temperatures at the three areas in and around Pele's Pit are significantly different at each area ($p < 0.001$), while $NO_3 + NO_2$ concentrations are significantly different between Pohaku and Hiolo
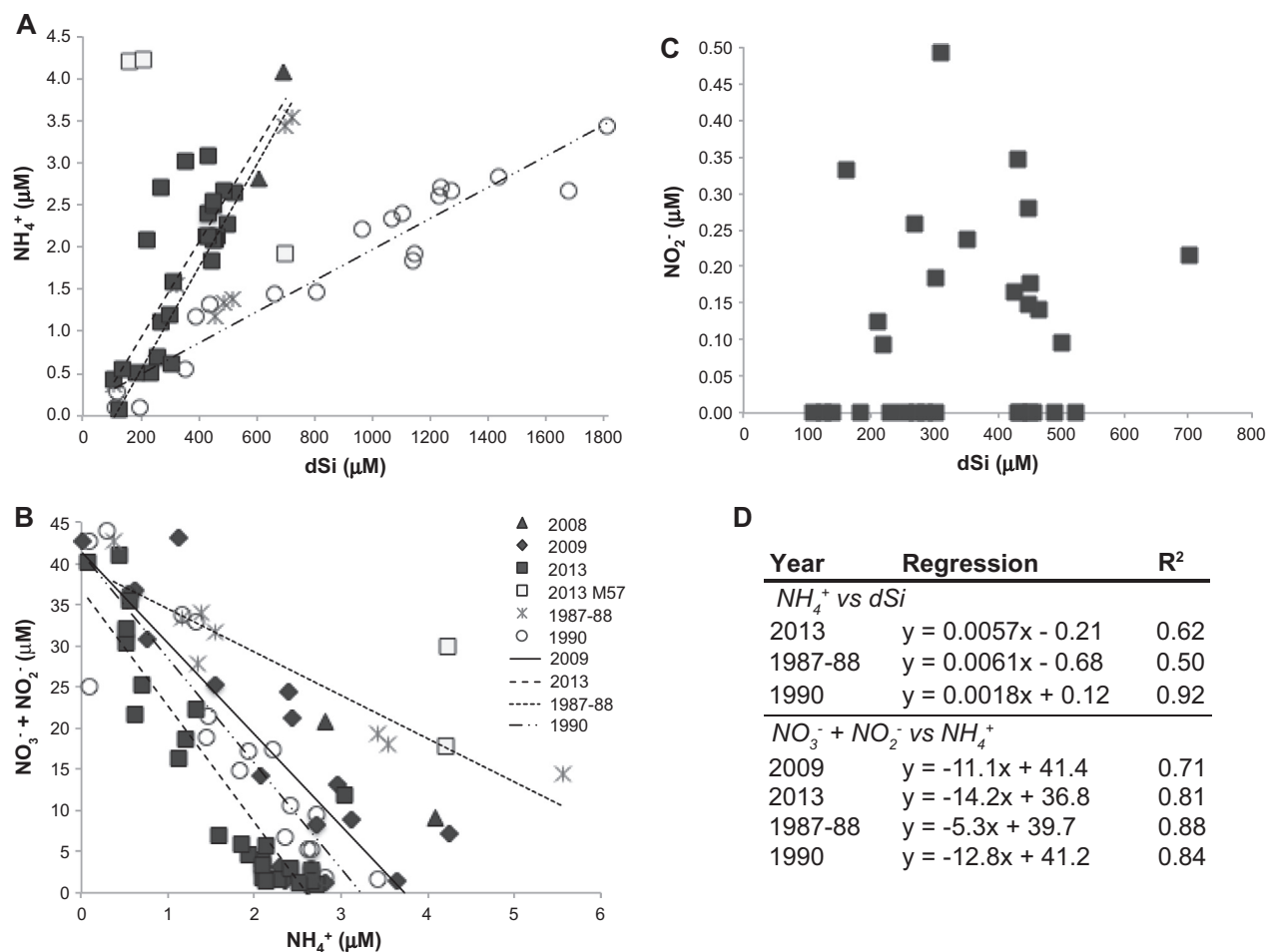
Fig. 3. Relationships between NH_4^+ and dSi (A), $NO_3 + NO_2$ and NH_4^+ (B) and NO_2^- and dSi (C). Regression lines and R^2 values for lines presented in A and B are given in (D). Pre-2008 data comes from Karl et al., 1989 (1987–88 data) and Sedwick et al., 1992 (1990 data). Data points from Karl et al. (1989) were limited to samples collected with Major samplers because samples collected with Niskin bottles opened over vents yielded significantly lower NH_4^+ and significantly higher $NO_3 + NO_2$ values by t-test.

Table 5
Kendall τ correlation values and significance for significantly correlated measured parameters, including data from 1987 to 88 (Karl et al., 1989), 1990 (Sedwick et al., 1992), 2008, 2009 and 2013.

Variable	By Variable	Kendall τ	Prob > |τ|
dSi	NH_4^+	0.3608	0.0003
dSi	$NO_3 + NO_2$	−0.2602	0.0083
$NO_3 + NO_2$	Temperature	−0.2529	0.0160
$NO_3 + NO_2$	NH_4^+	−0.3734	<0.0001
NO_2^-	Temperature	−0.5510	0.0073
P_i	Temperature	0.2857	0.0091
P_i	$NO_3 + NO_2$	−0.1986	0.0266

North ($p = 0.0114$), and P_i concentrations are significantly different between Hiolo South and Pohaku ($p = 0.0283$). NH_4^+ and dSi concentrations were not significantly variable between any of the three Pele's Pit sites.

While linear regressions are stronger when each year is considered independently (Fig. 3), significant correlations remain even when pooling all data points from both this work and earlier studies (Karl et al., 1989; Sedwick et al.,

1992), as shown in Table 5. Significant positive correlations exist between dSi and NH_4^+, while significant negative correlations exist between dSi and $NO_3 + NO_2$, between $NO_3 + NO_2$ and temperature, between NH_4^+ and $NO_3 + NO_2$, between NO_2^- and temperature and between P_i and $NO_3 + NO_2$.

3.2. Stable isotope measurements

Background seawater from depths of ∼1100 m (near Pele's Pit) had $\delta^{15}N_{NO_3}$ of +6.3‰ and $\delta^{18}O_{NO_3}$ of +3.2‰ (Table 6). Low-temperature vent fluid samples (up to ∼45 °C) collected from Pele's Pit generally exhibited increasing isotope ratios with decreasing concentrations of NO_3^- (Fig. 4a), with $\delta^{15}N$ ranging from +5.8 up to +11.5‰ and $\delta^{18}O$ from +4.0 up to +18.0‰. The changes in $\delta^{18}O_{NO_3}$ values were notably larger than the corresponding changes in $\delta^{15}N_{NO_3}$ values with respect to seawater (Fig. 4b), consistent with active cycling of N (see below). Vent plume samples collected from Pele's Pit in 2009 showed NO_3^- isotopic compositions that were largely indis-

Table 6

Isotopic composition for vent fluids, background seawater and water column profiles from Loihi Seamount. Temperature and nutrient data are as reported in Table 1. For some samples, $\delta^{15}N\text{-}NH_4^+$ could not be calculated because the mass balance based calculations yielded errors too large to report; these are labeled [*]. Isotopic composition for samples with no error reported were calculated a single time due to low sample volume.

Site	Sample	Temp (°C)	NH_4^+	$\delta^{15}N\text{-}NH_4^+$	NO_2^-	$NO_3 + NO_2$	$\delta^{15}N\text{-}NO_3^-$	$\delta^{18}O\text{-}NO_3^-$	dSi
Vent fluids									
M31	675-MS-black2	41.3	2.278	7.5	0.095	1.55	9.6	12.9	500.6
M31	672-MS-yellow	40.7	2.096	14.0 ± 1.3	0.093	1.86	8.7	16.1	218.6
M31	675-MS-red2	41.3	2.122	5.5 ± 1.1	0.142	1.51	11.5	15.2	464.6
M39	674-MS-black	25.7	1.122	[*]	0.259	16.34	6.4 ± 0.5	3.1 ± 1.1	268.6
Upper M31	674-MS-yellow	–	1.584	[*]	0.493	6.86	6.5 ± 0.3	6.2 ± 0.7	310.6
47 deg site	672-MS-black	47.1	2.721	4.8 ± 0.7	bd	1.05	9.4	15.2	270.6
Directly above M31, near M39, same site as 676-MS-white, in orifice	676-MS-yellow	41.2	2.096	0.0 ± 1.5	bd	4.02	6.4 ± 0.0	4.5 ± 0.4	456.6
Texture Garden (between M31 & M39)	676-MS-black	30.8	3.032	3.3 ± 2.5	0.236	11.82	6.2 ± 0.4	4.8 ± 0.8	352.6
Hiolo South area									
M38	675-MS-white	43.3	2.408	9.2 ± 1.2	bd	2.91	5.2 ± 0.1	4.3 ± 0.2	432.6
M38	675-MS-yellow	42.4	2.647	9.6 ± 1.1	bd	2.67	5.9 ± 0.6	8.7 ± 1.8	522.6
M34	675-MS-black	47.4	1.925	12.0 ± 1.9	0.215	4.53	–	–	700.6
M34	675-MS-yellow2	48.2	2.660	–	bd	1.38	9.8	18.0	488.6
M34	675-MS-red	47.4	0.705	[*]	bd	25.21	6.0 ± 0.3	2.7 ± 0.7	256.6
M34	675-MS-white2	48.1	2.508	4.8 ± 1.0	bd	1.16	11.4	20.2	450.6
Pohaku area									
M57	671-MS-white	25.9	4.211	[*]	0.333	17.70	6.1 ± 0.6	3.2 ± 1.2	160.6
Ula Nui area									
Ula Nui Mat	477-MS-blue	2.8	1.555	–	–	25.27	5.0 ± 0.3	2.1 ± 0.4	–
Background seawater									
M57 SW	476-niskin	5	0.015	–	–	42.61	6.2 ± 0.5	3.5 ± 0.5	–
Ula Nui SW	477-niskin	2.6	0.560	–	–	36.31	5.0 ± 0.1	2.9 ± 0.4	–
Water column profiles									
Pele's Pit CTD cast									
Pele's Pit, 2009	0901-16	4.0	1.200	–	–	36.45	7.3 ± 0.3	5.3 ± 0.3	36.5
Pele's Pit, 2009	0901-14	3.7	0.690	–	–	42.76	6.9 ± 0.2	3.8 ± 0.1	42.8
Tow-yo west of summit									
SW of Loihi	0904-02	3.7	0.286	–	–	41.79	6.2 ± 0.7	2.8 ± 0.2	108.8
SW of Loihi	0904-11	3.6	0.324	–	–	28.44	6.5 ± 0.7	3.6 ± 0.1	85.8
SW of Loihi	0904-15	3.7	0.167	–	–	41.41	6.5 ± 0.5	3.9 ± 0.7	95.8
SW of Loihi	0904-22	3.4	0.213	–	–	41.60	8.0 ± 0.2	6.0 ± 0.3	120.8
Pit of death CTD cast									
Pit of death, 2009	0905-19	3.9	0.076	–	–	47.22	7.8 ± 0.4	4.9 ± 0.3	101.8
Pit of death, 2009	0905-01	3.7	1.500	–	–	45.28	6.3 ± 0.5	4.1 ± 0.1	105.8
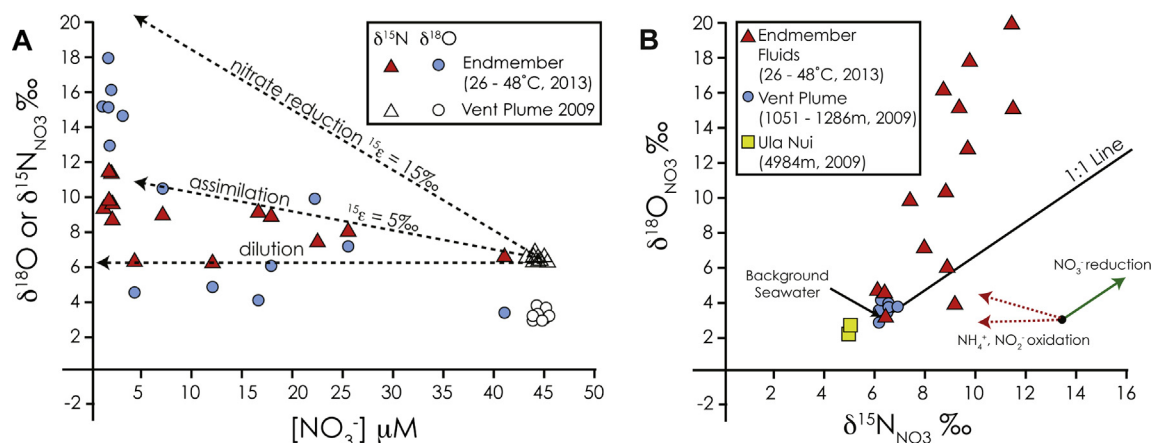
Fig. 4. $\delta^{15}N$ and $\delta^{18}O$ isotopic ratios in NO_3^- in Loihi fluids. Plot of $\delta^{15}N$-NO_3^- and $\delta^{18}O$-NO_3^- versus concentrations of NO_3^- (A) and $\delta^{15}N$-NO_3^- versus $\delta^{18}O$-NO_3^- (B).

tinguishable from background seawater, with $\delta^{15}N_{NO_3}$ values ranging from +5.7 to +6.4‰ (mean = +6.0 ± 0.2‰) and $\delta^{18}O_{NO_3}$ values ranging from +2.6 to +3.6‰ (mean = +3.1 ± 0.3‰). The two samples collected at Ula Nui (4984 m) were distinctly different from those collected from Pele's Pit, having lower $\delta^{15}N_{NO_3}$ and $\delta^{18}O_{NO_3}$ values of +5.0‰ and 2.4‰, respectively.

Nitrogen isotopes of ammonium were measured on a subset of hydrothermal fluid samples (Table 6). Because NH_4^+ isotopic composition is calculated by mass balance, we only report samples in which the fraction of NH_4^+ to the total inorganic N pool was at least 20% to minimize error propagation. $\delta^{15}N_{NH4}$ values range from 0.0‰ to +16.7‰, with no observed correlation to NH_4^+ concentration or temperature across the sampling sites (not shown). Notably, the majority of $\delta^{15}N_{NH4}$ values were near seawater NO_3^- values or higher, with only two values exhibiting lower values of 0.0‰ and +3.3‰.

3.3. Energy availability

The amount of energy available from the 17 reactions listed in Table 3 were calculated for hydrothermal fluids that are characteristic of three locations in Pele's Pit, Hiolo South, Pohaku and Hiolo North, and for three depths in a microbial mat sampled at the Ula Nui site (see Table 4 for compositions). Because most of the reactions shown in Table 3 yield a very small amount of energy, only the six most exergonic reactions are shown in Fig. 5. The amount of energy available from each of the reactions varies at each site (note that the scales in panels A and B in Fig. 5 are not the same). Under low energy conditions, Fig. 5A, iron oxidation coupled to nitrate reduction are among the most energy-dense reactions at Pohaku and in the top two parts of the Ula Nui mat. For the other sites under low-energy conditions, sulfide oxidation coupled to nitrate reduction reaction has the highest potential for microbial catabolism. For the high energy scenario, sulfide oxidation by nitrate has more potential than Fe oxidation at the Hiolo sites, while iron oxidation coupled to nitrate reduction has more potential to fuel microorganisms at the remaining sites.

Fe^{2+}, H_2S and NH_4^+ are the most significant electron donors in this environment, and NO_3^- is the oxidant that yields the most energy. Reactions in which CH_4 is the electron donor and nitrite the electron acceptor yield so little energy that they would not be visible in Fig. 5. Fluids sampled at Pohaku have the greatest potential for nitrogen-based catabolic activities under the low energy scenario, but rank third behind the Hiolo sites under the high energy scenario. The broad concentration ranges of electron donors and acceptors at the Hiolo sites result in these two sites having the highest and lowest energy densities in the high and low energy scenarios, respectively.

Of the six reactions presented in Fig. 5, three are described as Fe^{2+} oxidation by NO_3^- (reactions (1)–(3) in Table 3). These reactions only differ with respect to the oxidation state of the product nitrogen species: NO_2^-, N_2 and NH_4^+. At all six sample sites, the $Fe^{2+} + NO_3^-$ reaction to $N_{2(aq)}$ (Reaction (2)) is the most energy yielding of these reactions. Similarly, for the $H_2S + NO_3^-$ reactions (Reactions (11)–(14) in Table 3), the reaction in which $N_{2(aq)}$ is the product species (Reaction (11)) is the most energy yielding of the sulfide oxidation reactions. N_2 was not measured during this work, but is inferred to be created in the subsurface as the deficit between the concentrations of $NO_3 + NO_2 + NH_4^+$ in the background seawater and that in the vent fluids, which is likely tens of μM.

3.4. Microbial diversity

Background seawater samples collected at 1100 m and 1700 m are comprised largely of Alpha-, Delta- and Gammaproteobacteria (Fig. 6). The Alphaproteobacterial orders Rhodobacterales, Rhodospirillales and the SAR11 group within the order Rickettsiales are abundant in these seawater samples, as are the SAR324 clade of Deltaproteobacteria and the Gammaproteobacterial orders Alteromonadales and Oceanospiralles. Archaeal communities in the background samples are comprised largely of Thaumarchaeota and Thermoplasmata.

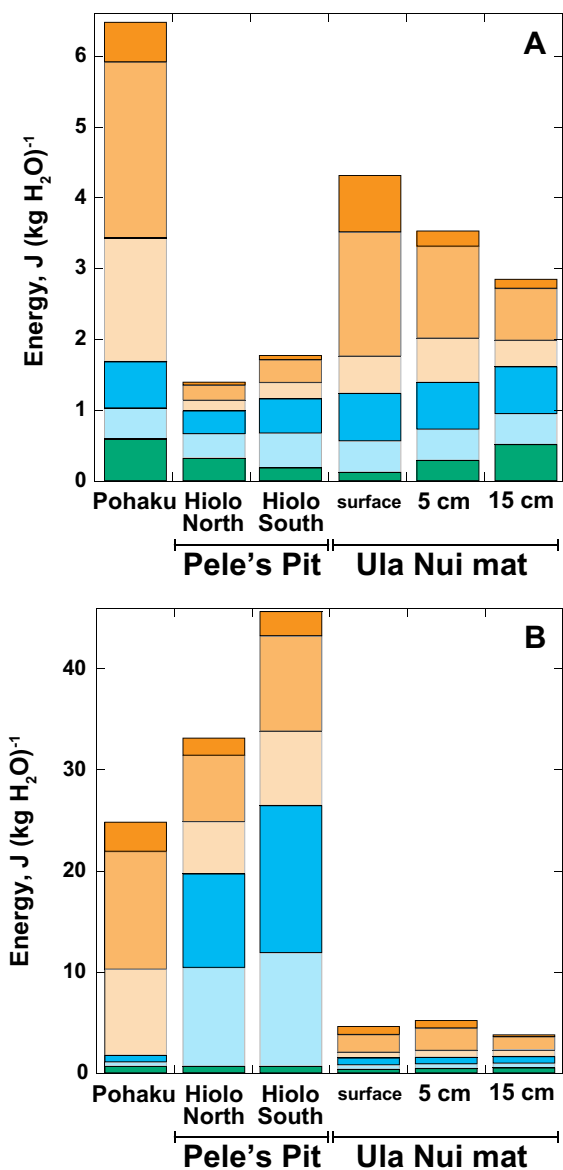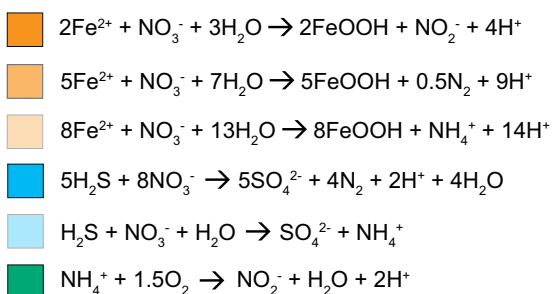Bacterial OTUs detected in Loihi fluids derive from 13 phyla and all 6 classes of Proteobacteria. OTUs classified

Reaction Key

$2Fe^{2+} + NO_3^- + 3H_2O \rightarrow 2FeOOH + NO_2^- + 4H^+$

$5Fe^{2+} + NO_3^- + 7H_2O \rightarrow 5FeOOH + 0.5N_2 + 9H^+$

$8Fe^{2+} + NO_3^- + 13H_2O \rightarrow 8FeOOH + NH_4^+ + 14H^+$

$5H_2S + 8NO_3^- \rightarrow 5SO_4^{2-} + 4N_2 + 2H^+ + 4H_2O$

$H_2S + NO_3^- + H_2O \rightarrow SO_4^{2-} + NH_4^+$

$NH_4^+ + 1.5O_2 \rightarrow NO_2^- + H_2O + 2H^+$

Fig. 5. Energy densities of microbially-mediated nitrogen redox reactions calculated using a low energy scenario (A) and a high energy scenario (B) for available substrates concentrations in Loihi fluids, as listed in Table 4. Only the six most exergonic reactions (those for which the energy density is >0.1 J (kg H₂O)⁻¹) are shown.

as Deltaproteobacteria in the order Syntrophobacterales are found in all three vent fluid samples from Pele's Pit, but not the sample LoihiPP6, collected at the Ula Nui site in 5000 m water depth. OTUs belonging to the order Thiotrichales within the γ-proteobacteria are abundant in LoihiPP2 (8.9%) and LoihiPP5 (5.4%), as are the OTUs within the Epsilon- (10.2% and 4.4%, respectively) and Zetaproteobacteria (13.1 and 10.1%, respectively) classes and the family Nitrospiraceae (18.9 and 19.2%, respectively). The genus *Thiohalophilus* is found in all three samples from Pele's Pit at relative abundances of 1.7–6.6% but represents only 0.11% of the pyrotags from Ula Nui. Finally, sequences belonging to the SAR406 clade within the Deferribacteres are common to all four diffuse flow samples (0.83–12.8%), and the thermophilic, anaerobic genus *Caldithrix* is common to the three samples from Pele's Pit (1.0–7.3%).

Archaeal OTUs common to Loihi subsurface fluids include the family Archaeoglobaceae (12.4–62.6% of all archaeal pyrotags), abundant in all three samples from Pele's Pit, and Marine Benthic Group E in the Thermoplasmata, which was common in all four samples (8.3–36.1%). The Halobacteria present in the Pele's Pit samples all derive from the order Halobacterales and either could not be classified further or belong to the Deep Sea Euryarcheotic Group. In LoihiPP1, Methanococci and Menthanomicrobia are present (3.4 and 12.3%, respectively), but these are absent from the other samples.

Among the prokaryotic OTUs detected in venting fluids, a portion of them belong to groups known to participate in nitrogen redox cycling. These are largely grouped into NO_3^- reduction/denitrification, N-fixation and NO_2^- oxidation (Fig. 6). Among these, the most abundant putative N-reducing microbes include *Caldithrix*, from which some members perform dissimilatory nitrate reduction to ammonium, or DNRA (Miroshnichenko et al., 2003), Epsilon-proteobacteria, *Thiohalophilus* and members of the SAR324 clade. Putative N-fixers detected include members of the bacterial order Chlorobiales and archaeal methanogens in the genera *Methanococcus* and *Methanothermococcus*. Members of the phylum Nitrospirae are present in all four samples, and are abundant in LoihiPP2 and LoihiPP5. Approximately 4 and 10% of the sequences were assigned to the genus Thermodesulfovibrio in LoihiPP2 and LoihiPP5, respectively, while only a few sequences, <1% in LoihiPP2 and none in LoihiPP5, were assigned to the genus *Nitrospira*. The majority of sequences classified as Nitrospirae could not be classified beyond Nitrospiraceae, therefore it is impossible to guess their role in N-cycling given that some members of this family are nitrite oxidizers (*Nitrospira*) while others are not (*Thermodesulfovibrio* and others).

It should be noted that OTUs from the genera *Marinobacter* and *Halomonas* and the NO_2^- oxidizing genus *Nitrospina* were abundant in fluid samples, but the same OTUs were detected in abundance in the background samples as well, and therefore do not appear in the background subtracted libraries reported (although different OTUs of *Marinobacter* not detected in the background samples are present). Both *Marinobacter* and *Halomonas* are cos-
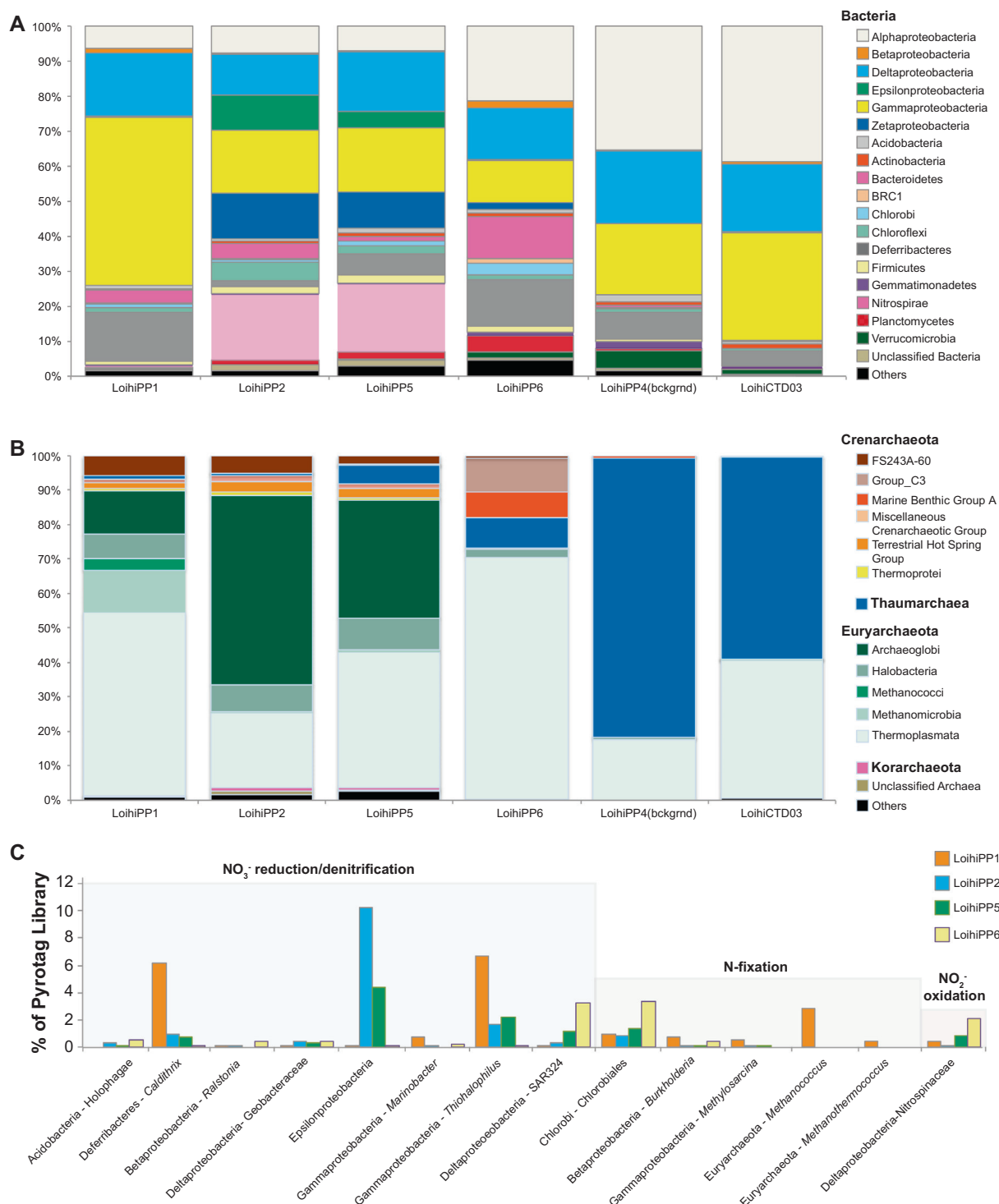
Fig. 6. Microbial communities in subsurface Loihi fluids. (A) Bacterial distributions. Data for LoihiPP1, LoihiPP2, LoihiPP5 and LohiPP6 are displayed with background OTUs detected in LoihiPP4 and LoihiCTD03 subtracted from them. (B) Archaeal distributions. Data for LoihiPP1, LoihiPP2, LoihiPP5 and LohiPP6 are displayed with background OTUs detected in LoihiPP4 and LoihiCTD03 subtracted from them. (C) Groups of putative N-redox cycling microbes detected in Loihi subsurface fluids. Bar heights represent percentage of total library from each of the four subsurface samples.

mopolitan genera common to both water column and sub-surface hydrothermal environments (Kaye et al., 2011) and therefore these OTUs are likely also present in the subsur-

face. Genes for nitrate reductase belonging to both genera have been detected in low temperature vent fluids and on active hydrothermal vent sulfides (Pérez-Rodríguez et al.,

2013a), and many isolates of *Marinobacter* (Takai et al., 2005) and hydrothermal vent derived isolates of *Halomonas* (Kaye et al., 2004) are NO_3^- reducers, lending further evidence to the likelihood that they are present and participating in NO_3^- reduction in both the water column and subsurface.

4. DISCUSSION

4.1. Biogeochemistry and isotope systematics at Loihi

While hydrothermally sourced Fe and CH_4 have been recognized as important energy sources for microbial metabolism at Loihi (Gamo et al., 1987; Emerson and Moyer, 2002), the role of N-redox transformations in supporting subsurface microbially mediated N-cycling is much less understood, in part due to the lack of measurements of inorganic N species at Loihi since the first studies that took place two decades ago (Karl et al., 1989; Sedwick et al., 1992). Those early studies of Loihi revealed elevated NH_4^+ in Loihi hydrothermal fluids in samples collected from Pele's vents prior to the July–August 1996 seismic events that resulted in the collapse of Pele's vents and the creation of the pit crater Pele's Pit (Hilton et al., 1998). Immediately following the creation of Pele's Pit, venting hydrothermal fluid temperatures reached 200 °C (Wheat et al., 2000), followed by a slow decrease in temperatures during 1997–1999 (Malahoff et al., 2006). Sampling of Loihi vents during 2006–2008 revealed that end-member fluid temperatures were 21–55 °C, similar to pre-1996 values (Glazer and Rouxel, 2009), and that Fe/Mn ratios returned to ∼30, the same as pre-1996 values (Glazer and Rouxel, 2009), indicative of a return to a steady state resembling pre-eruption conditions. Our hydrothermal fluid NH_4^+ data is similar in range to that of the earlier work (Fig. 3) and is in agreement with a return to steady state at Loihi. We also measured NO_2^- concentrations at Loihi for the first time. Concentrations were below detection for half of the samples collected and ∼0.10–0.50 μM for the rest. Although low, these levels of NO_2^- are consistent with active redox cycling involving NO_2^- as a product of NH_4^+ oxidation and/or NO_3^- reduction, both reactions that are favorable under *in situ* conditions (Fig. 5).

Concentrations of $NO_3 + NO_2$ and NH_4^+ in Loihi fluids are strongly negatively correlated (Fig. 3, Table 5), suggesting linkages between the redox cycling of these inorganic nitrogen species. These linkages may be the result of simultaneous abiotic and biotic mechanisms in Loihi's subsurface, with neither possibility being mutually exclusive. NO_3^- can be reduced abiotically to NH_4^+ with Fe^{2+} as a catalyst between 22 °C and 200 °C (Summers and Chang, 1993; Ottley et al., 1997; Smirnov et al., 2008; Holm and Neubeck, 2009) and therefore could be favorable in Loihi's subsurface environment. In addition to biologically mediated dissimilatory N-redox cycling, discussed below, biological assimilation can also have an effect on N-isotope composition in hydrothermal environments (Lee and Childress, 1994).

Unlike NH_4^+, NO_2^- shows no correlation to $NO_3 + NO_2$ or dSi. The lack of correlation with dSi suggests that it is of

low-temperature origin, likely released as a reactive intermediate of a biological process (i.e., not an endmember product of high temperature reactions). As NO_2^- is an intermediate of both denitrification and nitrification, the lack of correlation with conservative and non-conserved tracers is not surprising. Given the abundance of Fe^{2+} in these fluids, the mixing zone where subsurface fluids meet the seafloor likely represents a kinetic battleground between Fe-oxide precipitation and microbial utilization of oxygen for oxidation of compounds including NH_4^+ and NO_2^-. In order to shed more light on the nature of N-cycling reactions occurring, we also examined the N and O stable isotopic composition of N-bearing species. To our knowledge, only one study has reported on coupled N and O stable isotope measurements in the context of biogeochemical cycling of nitrogen species in a deep-sea hydrothermal system (Bourbonnais et al., 2012a). Using samples from the Endeavour Segment and Axial Volcano on the Juan de Fuca Ridge, these authors found evidence for removal of NO_3^- from fluids primarily by dissimilatory processes when NH_4^+ concentrations were ⩽10 μM, conditions representative of their diffuse flow sites as well as at those sampled at Loihi. Indeed, in a related study using ^{15}N isotope labeling, Bourbonnais et al. (2012a) observed the highest rates of nitrogen removal from these same sites, confirming the importance of reductive nitrate consumption. In addition to evidence for cycling involving NO_3^-, Bourbonnais et al. (2012a) also found evidence for both consumption and production of NH_4^+ by microbial activity. This important initial work indicated that microbial denitrification is a primary route of inorganic nitrogen loss in diffuse fluids, but also noted possible spatial and temporal heterogeneity in N redox processes. However, the sites on the Juan de Fuca Ridge and Axial Seamount exhibit high concentrations of sulfide, which strongly influence the composition of the resident microbial communities. In contrast, fluids from Loihi Seamount, with low sulfide and high iron, represent a starkly different geochemical context for low-temperature venting.

Hydrothermal fluids having NO_3^- concentrations lower than background seawater can stem from either abiotic or biological consumption of NO_3^-, as mentioned above, or from dilution of fluids containing little or no NO_3^-. While dilution would have no influence on isotopic composition, isotope fractionation by biological reduction of nitrate leads to increases in both $\delta^{15}N$ and $\delta^{18}O$ of the remaining nitrate pool (Granger et al., 2008), allowing one to discern between biological consumption and physical mixing processes. Indeed, nitrate reduction, whether by dissimilatory or assimilatory processes, has been shown to impart distinctly parallel (e.g. equal) isotope effects for both N and O, leading to a characteristic 1:1 dual isotopic evolution (e.g., slope of 1 in Fig. 4). The elevated N and O isotope ratios of NO_3^- in the hydrothermal fluids of Pele's Pit clearly reflect the influence of biological NO_3^- consumption. However, in contrast to the parallel 1:1 increases in $\delta^{15}N_{NO_3}$ and $\delta^{18}O_{NO_3}$ (relative to the composition of background seawater) expected from isotopic fractionation due to NO_3^- consumption alone, changes in the $\delta^{18}O_{NO_3}$ values are

much larger than changes in $\delta^{15}N$ values, suggesting that processes other than NO_3^- reduction are also occurring. Indeed, such deviations from a 1:1 covariation in dual isotope space for NO_3^- have been observed in other marine systems including oxygen minimum zones (Sigman et al., 2005; Casciotti and McIlvin, 2007; Bourbonnais et al., 2012a), shallow surface water environments (e.g., Wankel et al., 2007) and even other deep biosphere environments (Wankel et al., 2015), and have been interpreted as reflecting the combined effects of NO_3^- consumption (via reduction) and NO_3^- regeneration (via nitrification). Results of a recent modeling study suggest that isotopic signatures of nitrification evident in denitrifying systems might be a universal characteristic of nitrogen cycling in aquatic systems (Granger and Wankel, 2016).

Given the prevalence of NH_4^+ in the hydrothermal fluids at Loihi, we suggest that the contribution of (1) partial NH_4^+ oxidation and (2) possibly rapid NO_2^- reoxidation leads to the observed deviation of NO_3^- dual isotopic composition from the 1:1 line (Fig. 4). This dynamic arises because N and O isotope enrichments in NO_3^- are tightly coupled during consumption (e.g. Granger et al., 2008), while the production of NO_3^- by nitrification (both ammonia oxidation to nitrite, as well as nitrite oxidation to nitrate) represents a unique decoupling of these two isotope systems as discussed further below (Casciotti and McIlvin, 2007; Wankel et al., 2007; Sigman et al., 2009). Foremost, under the mesophilic conditions at the Loihi vents, the partial oxidation of the NH_4^+ pool by ammonia oxidizing microbes, which is known to have a large N isotope effect (14–38‰; (Casciotti et al., 2003; Santoro and Casciotti, 2011)), would result in production of low $\delta^{15}N_{NO_3}$. Indeed, the occurrence of elevated $\delta^{15}N_{NH_4}$ values in Loihi fluids (up to +16‰), strongly supports that oxidative processes have partially consumed the vent derived NH_4^+ pool. While it is impossible to accurately estimate the $\delta^{15}N_{NO_3}$ of newly produced NO_3^- from a partially oxidized NH_4^+ pool using the existing data (i.e., it is difficult to estimate the fraction of NH_4^+ consumed at these low concentrations and the isotope effects for NH_4^+ oxidation range quite widely (Casciotti et al., 2003)), it is clear that the contribution of this newly produced NO_3^- having a very low $\delta^{15}N$ value would act to shift the bulk NO_3^- dual isotopic composition to the left of the 1:1 line evolving from a background seawater source (Fig. 4).

The oxygen isotope composition of newly produced NO_3^- may also play a role in the observed deviation from the 1:1 line, specifically implicating nitrite oxidation (and nitrite oxidizing bacteria). The source O atoms of new NO_3^- originate from both H_2O and O_2 (Buchwald and Casciotti, 2010; Casciotti et al., 2010) with kinetic isotope effects at each step of O atom incorporation as well as the potential for oxygen isotope equilibration between the NO_2^- intermediate pool and water (Casciotti and McIlvin, 2007; Buchwald and Casciotti, 2013). In general, it is believed that the combination of these influences results in the $\delta^{18}O$ of newly produced NO_3^- to be near $+1.9 \pm 3‰$ in seawater (Buchwald et al., 2012). Given the low pH of the Loihi fluids, ~5.7–6.5 (Glazer and

Rouxel, 2009), it is safe to assume that the $\delta^{18}O$ of the intermediate nitrite pool (whether derived from NH_4^+ oxidation or NO_3^- reduction) is in isotopic equilibrium with the ambient water – which would yield a value of ~14‰ (Casciotti and McIlvin, 2007). During partial oxidation of this NO_2^- pool, the kinetic isotope effects associated with both NO_2^- oxidation ($^{18}\varepsilon_{nxr,NO2}$) as well as incorporation of an O atom from H_2O ($^{18}\varepsilon_{nxr,H2O}$), would culminate in production of new NO_3^- with a $\delta^{18}O$ value of between +4 and +12‰ (see Buchwald and Casciotti, 2010), higher than that of background seawater. In support of this mechanism, our data reveal the presence of known nitrite-oxidizing genera in the family Nitrospinaceae. As indicated in Fig. 6, the combination of NO_3^- reduction by denitrifying microbes together with nitrification (both the partial oxidation of the NH_4^+ pool as well as the reoxidation of NO_2^-) act in opposing directions, modulating the evolving NO_3^- dual isotopic composition to fall above the 1:1 line predicted by denitrification alone. Co-occurring denitrification and nitrification was found to occur in Beggiatoa mats in Guaymas Basin (Winkel et al., 2014), indicating this may be a widespread feature in hydrothermal systems hosting sharp gradients of oxygen and nitrogen species. In summary, our data clearly suggest that both microbially mediated reductive and oxidative processes play a joint role in regulating fluxes of dissolved inorganic nitrogen from the Loihi subsurface. Although hydrothermal vent N isotope data is sparse, such NO_3^- dual isotope dynamics have also been recently observed in other hydrothermal systems (Bourbonnais et al., 2012a), reflecting the simultaneous influence of a range of redox reactions at a sharp fluid-mixing zone. Importantly, the data from Loihi reveals that this range of redox reactions also occurs in a hydrothermal system with low concentrations of dissolved H_2S and high concentrations of dissolved Fe^{2+}. This indicates that the presence or absence of H_2S and metabolisms coupling H_2S and N-redox transformations do not greatly alter the N-isotope systematics in diffuse flow hydrothermal vent environments. The precise cause requires more study, but may reflect substitution of N-redox processes coupled with H_2S oxidation with other oxidative processes (Fe^{2+} oxidation, for example), that H_2S is more important in the subsurface biosphere at Loihi but not abundant as measured in samples collected at the seafloor, or that H_2S is not a strong influence on N-redox processes.

We note also that the NO_3^- dual isotope values from Ula Nui are slightly lower in $\delta^{15}N$ and $\delta^{18}O$ than background waters near the Pele's Pit crater and look more similar to background seawater than vent fluids. A likely scenario explaining these data is that the water in the matrix of the mats at the Ula Nui site is derived more from deep seawater than the ultra diffuse fluids emanating from the seafloor at that site (Edwards et al., 2011).

4.2. Energetics from N-redox reactions in the Loihi subsurface

Microorganisms are known to catalyze nitrogen redox reactions in order to gain energy (see Amend and Shock

(2001) for a review). The amount of energy available from these reactions depends on the temperature, pressure and concentrations of all of the chemical species in the reactions describing a particular catabolic pathway. Because the temperatures and composition of the hydrothermal fluids at Loihi change with time, the calculations presented here were carried out under high and low energy conditions in order to capture this variability and to reflect the reality that fluid flow rates, the paths that hydrothermal fluids take in the subsurface, and the extent to which they mix with seawater is variable. However, we can only carry out our analyses/calculations based on the samples that we obtained, which are snapshots in time that reflect at least a few realities for this system. The total amount of energy available from the individual nitrogen redox reactions shown in Fig. 5 for low energy conditions is less than $\sim$7 J $(kg\ H_2O)^{-1}$. Energy densities under more favorable conditions total 4–46 J $(kg\ H_2O)^{-1}$. The magnitude of this potential can be understood by comparing it to other studies that have presented the energetic potential of redox reactions in units of energy densities and by considering how much energy microorganisms demand. Most studies that present energetic analyses of potential microbial metabolisms in units of energy densities do so because they are quantifying the disequilibrium resulting from the mixing of seawater with hydrothermal fluids (McCollom and Shock, 1997; Amend et al., 2011). Because the composition of hydrothermal fluids can vary dramatically depending upon the types of rocks that the hydrothermal fluids circulate through, the resulting amount of redox energy that can be available for microbial processes varies considerably. For instance, fluids from ultramafic hydrothermal systems that mix with seawater can provide up to 3700 J $(kg\ H_2O)^{-1}$ for H_2 oxidation with O_2 as the electron acceptor (McCollom, 2007), while seawater mixing with basalt-derived fluids at a mid-ocean ridge system (East Pacific Rise, EPR, 21° N OBS vent) only makes about $\sim$35 J $(kg\ H_2O)^{-1}$ available for the same reaction (Shock and Holland, 2004). On the other end of the spectrum, potential energy yields for some reactions due to fluid mixing can be less than 10^{-4} J $(kg\ H_2O)^{-1}$ (Price et al., 2015). The larger values noted above are likely outliers for most natural systems since they are capturing the mixing of two radically distinct fluids instantaneously. In environmental settings that are not subjected to such dramatic gradients, the energy densities are on par or smaller than those shown in Fig. 5. (LaRowe et al., 2014; Osburn et al., 2014; Teske et al., 2014; Price et al., 2015).

All of the reactions whose energy densities are shown in Fig. 5 supply more than 0.1 J $(kg\ H_2O)^{-1}$. Although this may not seem like a large amount of energy, it is worth noting that maintenance energies for microorganisms range from 0.019 to 4700×10^{-15} J $(s\ cell)^{-1}$ (LaRowe and Amend, 2015). This means that a community of 10^6 cells could be supported on a typical maintenance level (e.g., 10^{-14} J $(s\ cell)^{-1}$) by any of the reactions considered at Loihi for almost 4 months using only the constituents of 1 liter of hydrothermal fluid. If 0.1 J $(kg\ H_2O)^{-1}$ were channeled into biomass synthesis, then between $\sim$10^7 and 10^9 cells could be produced, depending on the sources of C,

N, S, the overall redox state and other physiochemical variables (LaRowe and Amend, 2016).

4.3. Microbial diversity in the Loihi subsurface

The temperatures of hydrothermal fluids at Loihi make it comparable to diffuse-flow hydrothermal sites at spreading centers and seamounts. However, unlike the majority of these systems, sulfide concentrations are only moderately elevated relative to background seawater at Loihi (Sedwick et al., 1992). Thus, perhaps not surprisingly, sulfur oxidizing Epsilonproteobacteria represent only 0.15–10.3% of the bacterial communities in the four subsurface fluid samples analyzed here (Fig. 6). In contrast, previous studies of diffuse hydrothermal fluids with high concentrations of H_2S found that Epsilonproteobacteria represented a large proportion of the total bacterial community (Huber et al., 2007, 2010; Bourbonnais et al., 2012b). For example, in fourteen samples of diffuse fluids venting at five different seamounts along the Mariana Arc, with one exception, Epsilonproteobacteria comprised 15–87% of the total bacterial community, with a mean value of 37.4% (Huber et al., 2010). At Axial volcano, on the Juan de Fuca Ridge, Epsilonproteobacteria comprise up to 80% of the total bacterial community (Huber et al., 2007; Bourbonnais et al., 2012b). In those studies, the major genera of Epsilonproteobacteria detected at each vent site were variable, but members of *Sulfurimonas*, *Sulfurovum* and *Hydrogenomonas* were predominant. *Sulfurimonas*, *Sulfurovum*, *Hydrogenomonas* and *Nitratiruptor* combined comprised >99% of the Epsilonproteobacteria sequences detected in the Loihi samples. Fluids from the area where LoihiPP2 and LoihiPP5 were collected were $\sim$50 °C, and contained little to no O_2 (below detection, or <3 μM) and $\sim$2–4 μM HS^- during the time of sampling (Glazer and Rouxel, 2009). These conditions are ideal for the Epsilonproteobacteria detected, while reduced sulfur compounds were below detection at the sites where they were not detected, Marker 34 and Ula Nui (Glazer and Rouxel, 2009; Edwards et al., 2011). Cultured representatives from all the Epsilonproteobacterial genera detected here are NO_3^- reducers with the conserved periplasmic nitrate reductase (*nap*) gene pathway for this process (Vetriani et al., 2014), suggesting their importance in NO_3^- reduction at Loihi. Despite their lower abundance than at other vent sites, Epsilonproteobacteria still represent the most abundant putative NO_3^- reducers. In addition to the Epsilonproteobacteria detected, other detected NO_3^- reducers or denitrifiers include Gammaproteobacteria in the genera *Thiohalophilus*, *Marinobacter* and *Halomonas* as well as the genus *Caldithrix*. While Gammaproteobacteria from the SUP05 clade were noted as abundant denitrifiers at Axial Volcano (Bourbonnais et al., 2012b), they were not detected at Loihi, likely due to the low abundance of H_2S. A related study detected heme-containing nitrite reductase (*nirS*) genes related to *Pseudomonas* spp. in diffuse flow hydrothermal vent fluids along the Endeavour Segment (Bourbonnais et al., 2014), but *Pseudomonas* were also not detected at abundances >0.3% in our hydrothermal fluids samples. *Pseudomonas* was detected in the background samples at abundances of

0.71 and 0.090% (samples LoihiPP4 and CTD03, respectively), and it is possible that overlap between these OTUs and those in hydrothermal fluids caused underrepresentation of *Pseudomonas* in the vent samples. Prior to OTU removal, pyrotags classified as *Pseudomonas* comprise 1.0, 0.70, 0.22 and 2.667% of all pyrotags in samples PP1, PP2, PP5 and PP6, respectively. Like *Marinobacter* and *Halomonas*, members of the genus *Pseudomonas* are cosmopolitan and likely to be found in both background seawater and hydrothermal fluid samples.

Among the few known archaeal denitrifiers are members of the genera *Halobacteria* and *Ferroglobus*, both in the Euryarchaeota (Offre et al., 2013). While the classes Halobacteria and Archaeoglobi were both abundant in Loihi fluids, there is not enough phylogenetic resolution in the V6 region of SSU rRNA to confidently assign the sequences recovered to one of the denitrifying genera. It is possible that members of the Thermoproteales are participating in denitrification at Loihi, although they were present in low abundances here. Recent metagenomic analysis revealed that members of the Thermoproteales possess genes in the *nir* and *nar* pathways, indicative of NO_3^- and NO_2^- reduction (Swingley et al., 2012). This group was present at 0.05, 0.22 and 0.20% relative abundance in the archaeal pyrotag libraries from Loihi PP1, PP2 and PP5, respectively, indicating a potential additional role for archaeal denitrification at Loihi by these organisms.

Putative N-fixing Bacteria and Archaea were detected in the Hiolo North area, although representing only a minor percentage of the entire population (Fig. 6). While some Archaea are known to participate in denitrification (Haroon et al., 2013; Offre et al., 2013), this is still a relatively underexplored metabolic pathway in Archaea. N_2 is likely abundant as indicated by the deficit between seawater $NO_3 + NO_2$ and the sum of measured N species in end-member fluids presented here, suggesting that N-fixation in low-temperature diffuse fluids at Loihi may be occurring. N-fixation in the warm Loihi subsurface environment is also suggested from two samples with $\delta^{15}N$ values lower than background seawater NO_3^- (0.0‰ and +3.3‰); remineralization of biomass supported by N-fixing microbes would generate NH_4^+ having $\delta^{15}N$ values near 0‰ (Delwiche and Steyn, 1970; Meador et al., 2007). It is also possible, however, that these values are indicative of low $\delta^{15}N$ produced NH_4^+ from DNRA, which has been shown to have an isotope effect of −6 to −8‰ in hydrothermal vent isolates (Perez-Rodriguez et al., 2013b) and which would therefore generate NH_4^+ with a $\delta^{15}N$ of between −2 and 0‰ from bottom seawater NO_3^- ($\delta^{15}N$ ∼+6‰).

4.4. Conclusions

The combined data presented here on biogeochemical measurements, isotope systematics, energetic calculations and microbial diversity present strong multidisciplinary data that N-cycling processes are occurring and likely biologically mediated in Loihi subsurface fluids, and that both oxidative and reductive processes are likely occurring simultaneously. A similar conclusion was drawn from the work of Bourbonnais and colleagues on the Juan de Fuca

Ridge (Bourbonnais et al., 2012a,b), and cryptic N-cycling was explicitly demonstrated in Beggiatoa mats in Guaymas Basin, where Beggiatoa perform denitrification in concert with attached nitrifiers (Winkel et al., 2014). Thus, there is a growing consensus that subsurface N-cycling processes are linked and complicated, but the role of N-cycling in driving subsurface biogeochemistry and microbiology is still underexplored.

Like Loihi, there are many hydrothermal systems with elevated concentrations of Fe^{2+} and low concentrations of sulfide around the globe, including the Marianas back-arc (Davis and Moyer, 2008) and diffuse vents along the Mid-Atlantic Ridge (Scott et al., 2014). Therefore, the work presented here can be interpreted to potentially represent high Fe, low sulfide systems elsewhere. Additionally, our results are in agreement with those derived from the Juan de Fuca Ridge and Axial Volcano, where sulfide is abundant (Bourbonnais et al., 2012a,b), indicating that trends presented here are potentially representative of low-temperature venting systems in general, which represent up to 90% of venting worldwide (Elderfield and Schultz, 1996).

REFERENCES

Amend J. P. and Shock E. L. (2001) Energetics of overall metabolic reactions of thermophilic and hyperthermophilic Archaea and Bacteria. *FEMS Microbiol. Rev.* **25**, 175–243.

Amend J. P., McCollom T. M., Hentscher M. and Bach W. (2011) Catabolic and anabolic energy for chemolithoautotrophs in deep-sea hydrothermal systems hosted in different rock types. *Geochim. Cosmochim. Acta* **75**, 5736–5748.

Bennett S. A., Hansman R. L., Sessions A. L., Nakamura K. and Edwards K. J. (2011) Tracing iron-fueled microbial carbon production within the hydrothermal plume at the Loihi seamount. *Geochim. Cosmochim. Acta* **75**, 5526–5539.

Bourbonnais A., Lehmann M. F., Butterfield D. A. and Juniper S. K. (2012a) Subseafloor nitrogen transformations in diffuse hydrothermal vent fluids of the Juan de Fuca Ridge evidenced by the isotopic composition of nitrate and ammonium. *Geochem. Geophys. Geosyst.* **13**, Q02T01.

Bourbonnais A., Juniper K., Butterfield A., Devol H., Kuypers M. M. M., Lavik G., Hallam J., Wenk B., Chang X., Murdock A. and Lehmann F. (2012b) Activity and abundance of denitrifying bacteria in the subsurface biosphere of diffuse hydrothermal vents of the Juan de Fuca Ridge. *Biogeosciences* **9**, 4661–4678.

Bourbonnais A., Juniper S. K., Butterfield D. A., Anderson R. E. and Lehmann M. F. (2014) Diversity and abundance of Bacteria and nirS-encoding denitrifiers associated with the Juan de Fuca Ridge hydrothermal system. *Ann. Microbiol.* **64**, 1691–1705.

Breier J. A., Gomez-Ibanez D., Reddington E., Huber J. A. and Emerson D. (2012) A precision multi-sampler for deep-sea hydrothermal microbial mat studies. *Deep Sea Res. Part I* **70**, 83–90.

Buchwald C. and Casciotti K. L. (2010) Oxygen isotopic fractionation and exchange during bacterial nitrite oxidation. *Limnol. Oceanogr.* **55**, 1064–1074.

Buchwald C., Santoro A. E., McIlvin M. R. and Casciotti K. L. (2012) Oxygen isotopic composition of nitrate and nitrite produced by nitrifying cocultures and natural marine assemblages. *Limnol. Oceangr.* **57**, 1361–1375.

Buchwald C. and Casciotti K. L. (2013) Isotopic ratios of nitrite as tracers of the sources and age of oceanic nitrite. *Nat. Geosci.* **6**, 308–313.

Byrne N., Strous M., Crépeau V., Kartal B., Birrien J. L., Schmid M., Lesongeur F., Schouten S., Jaeschke A., Jetten M., Prieur D. and Godfroy A. (2009) Presence and activity of anaerobic ammonium-oxidizing bacteria at deep-sea hydrothermal vents. *ISME J.* **3**, 117–123.

Casciotti K. L., Sigman D. M., Hastings M. G., Böhlke J. K. and Hilkert A. (2002) Measurement of the oxygen isotopic composition of nitrate in seawater and freshwater using the denitrifier method. *Anal. Chem.* **74**, 4905–4912.

Casciotti K. L., Sigman D. M. and Ward B. B. (2003) Linking diversity and stable isotope fractionation in Ammonia-Oxidizing Bacteria. *Geomicrobiol. J.* **20**, 335–353.

Casciotti K. L. and McIlvin M. R. (2007) Isotopic analyses of nitrate and nitrite from reference mixtures and application to Eastern Tropical North Pacific waters. *Mar. Chem.* **107**, 184–201.

Casciotti K. L., McIlvin M. and Buchwald C. (2010) Oxygen isotopic exchange and fractionation during bacterial ammonia oxidation. *Limnol. Oceanogr.* **55**, 753–762.

Cole J. R., Wang Q., Cardenas E., Fish J., Chai B., Farris R. J., Kulam-Syed-Mohideen A. S., McGarrell D. M., Marsh T., Garrity G. M. and Tiedje J. M. (2009) The Ribosomal Database Project: improved alignments and new tools for rRNA analysis. *Nucleic Acids Res.* **37**, D141–D145.

Davis R. E. and Moyer C. L. (2008) Extreme spatial and temporal variability of hydrothermal microbial mat communities along the Mariana Island Arc and southern Mariana back-arc system. *J. Geophys. Res. Solid Earth* **113**, B08S15.

Delwiche C. C. and Steyn P. L. (1970) Nitrogen isotope fractionation in soils and microbial reactions. *Environ. Sci. Technol.* **4**, 929–935.

Dittmar T., Koch B., Hertkorn N. and Kattner G. (2008) A simple and efficient method for the solid-phase extraction of dissolved organic matter (SPE-DOM) from seawater. *Limnol. Oceanogr.: Methods* **6**, 230–235.

Edwards K. J., Glazer B. T., Rouxel O. J., Bach W., Emerson D., Davis R. E., Toner B. M., Chan C. S., Tebo B. M., Staudigel H. and Moyer C. L. (2011) Ultra-diffuse hydrothermal venting supports Fe-oxidizing bacteria and massive umber deposition at 5000 m off Hawaii. *ISME J.* **5**, 1748–1758.

Elderfield H. and Schultz A. (1996) Mid-ocean ridge hydrothermal fluxes and the chemical composition of the ocean. *Annu. Rev. Earth Planet. Sci.* **24**, 191–224.

Emerson D. and Moyer C. L. (2002) Neutrophilic Fe-Oxidizing bacteria are abundant at the Loihi Seamount hydrothermal vents and play a major role in Fe oxide deposition. *Appl. Environ. Microbiol.* **68**, 3085–3093.

Gamo T., Ishibashi J. I., Sakai H. and Tilbrook B. (1987) Methane anomalies in seawater above the Loihi submarine area, Hawaii. *Geochim. Cosmochim. Acta* **51**, 2857–2864.

Garside C. (1982) A chemiluminescent technique for the determination of nanomolar concentrations of nitrate and nitrite in seawater. *Mar. Chem.* **11**, 159–167.

Gieskes J. M., Gamo T., Brumsack H. (1991) Chemical methods for interstitial water analysis aboard JOIDES Resolution. ODP Technical Note 15, College Station, TX (Ocean Drilling Program).

Glazer B. T. and Rouxel O. J. (2009) Redox speciation and distribution within diverse iron-dominated microbial habitats at Loihi Seamount. *Geomicrobiol. J.* **26**, 606–622.

Granger J., Sigman D. M., Lehmann M. F. and Tortell P. D. (2008) Nitrogen and oxygen isotope fractionation during dissimilatory nitrate reduction by denitrifying bacteria. *Limnol. Oceanogr.* **53**, 2533–2545.

Granger J. and Sigman D. M. (2009) Removal of nitrite with sulfamic acid for nitrate N and O isotope analysis with the denitrifier method. *Rapid Commun. Mass Spectrom.* **23**, 3753–3762.

Granger J. and Wankel S. D. (2016) Isotopic overprinting of nitrification on denitrification as a ubiquitous and unifying feature of environmental nitrogen cycling. *Proc. Natl. Acad. Sci. U.S.A.* **113**, E6391–E6400.

Grasshoff K., Kremling K. and Ehrhardt M. (1999) *Methods of Seawater Analysis*, 3rd ed. Wiley-Vch, Weinheim.

Haroon M. F., Hu S., Shi Y., Imelfort M., Keller J., Hugenholtz P., Yuan Z. and Tyson G. W. (2013) Anaerobic oxidation of methane coupled to nitrate reduction in a novel archaeal lineage. *Nature* **500**, 567–570.

Helgeson H. C. (1969) Thermodynamics of hydrothermal systems at elevated temperatures and pressures. *Am. J. Sci.* **267**, 729–804.

Helgeson H. C., Kirkham D. H. and Flowers G. C. (1981) Theoretical prediction of the thermodynamic behavior of aqueous electrolytes by high pressures and temperatures; IV, Calculation of activity coefficients, osmotic coefficients, and apparent molal and standard and relative partial molal properties to 600 degrees C and 5 kb. *Am. J. Sci.* **281**, 1249–1516.

Hilton D. R., McMurtry G. M. and Goff F. (1998) Large variations in vent fluid CO_2/He-3 ratios signal rapid changes in magma chemistry at Loihi seamount, Hawaii. *Nature* **396**, 359–362.

Holmes R. M., Aminot A., Kerouel R., Hooker B. A. and Peterson B. J. (1999) A simple and precise method for measuring ammonium in marine and freshwater ecosystems. *Can. J. Fish. Aquat. Sci.* **56**, 1801–1808.

Holm N. G. and Neubeck A. (2009) Reduction of nitrogen compounds in oceanic basement and its implications for HCN formation and abiotic organic synthesis. *Geochem. Trans.* **10**, 9.

Huber J. A., Mark Welch D., Morrison H. G., Huse S. M., Neal P. R., Butterfield D. A. and Sogin M. L. (2007) Microbial population structures in the deep marine biosphere. *Science* **318**, 97–100.

Huber J. A., Cantin H. V., Huse S. M., Welch D. B. M., Sogin M. L. and Butterfield D. A. (2010) Isolated communities of Epsilonproteobacteria in hydrothermal vent fluids of the Mariana Arc seamounts. *FEMS Microbiol. Ecol.* **73**, 538–549.

Huse S. M., Dethlefsen L., Huber J. A., Welch D. M., Relman D. A. and Sogin M. L. (2008) Exploring microbial diversity and

taxonomy using SSU rRNA hypervariable tag sequencing. *PLoS Genet.* **4**.

Huse S. M., Welch D. M., Morrison H. G. and Sogin M. L. (2010) Ironing out the wrinkles in the rare biosphere through improved OTU clustering. *Environ. Microbiol.* **12**, 1889–1898.

Jesser K. J., Fullerton H., Hager K. W. and Moyer C. L. (2015) Quantitative PCR analysis of functional genes in iron-rich microbial mats at an active hydrothermal vent system (Lō'ihi Seamount, Hawai'i). *Appl. Environ. Microbiol.* **81**, 2976–2984.

Johnson J. W., Oelkers E. H. and Helgeson H. C. (1992) SUPCRT92 – a software package for calculating the standard molal thermodynamic properties of minerals, gases, aqueous species, and reactions from 1-bar to 50,000-bar and 0-degrees-C to 1000-degrees-C. *Comput. Geosci.* **18**, 899–947.

Karl D. M., McMurtry G. M., Malahoff A. and Garcia M. O. (1988) Loihi Seamount, Hawaii: a mid-plate volcano with a distinctive hydrothermal system. *Nature* **335**, 532–535.

Karl D. M., Brittain A. M. and Tilbrook B. D. (1989) Hydrothermal and microbial processes at Loihi Seamount, a mid-plate hot-spot volcano. *Deep-Sea Res. Part A – Oceanogr. Res. Pap.* **36**, 1655–1673.

Kaye J. Z., Marquez M. C., Ventosa A. and Baross J. A. (2004) *Halomonas neptunia* sp. nov, *Halomonas sulfidaeris* sp. nov., *Halomonas axialensis* sp nov and *Halomonas hydrothermalis* sp. nov.: halophilic bacteria isolated from deep-sea hydrothermal-vent environments. *Int. J. Syst. Evol. Microbiol.* **54**, 499–511.

Kaye J. Z., Sylvan J. B., Edwards K. J. and Baross J. A. (2011) *Halomonas* and *Marinobacter* ecotypes from hydrothermal-vent, subseafloor and deep-sea environments. *FEMS Microbiol. Ecol.* **75**, 123–133.

Knapp A. N., Sigman D. M. and Lipschultz F. (2005) N isotopic composition of dissolved organic nitrogen and nitrate at the Bermuda Atlantic Time-series Study site. *Global Biogeochem. Cycles* **19**, GB1018.

LaRowe D. E., Amend J. P., Kallmeyer J. and Wagner D. (2014) Energetic constraints on life in marine deep sediments. *Life Extreme Environ.: Microb. Life Deep Biosphere*, 279–302.

LaRowe D. E. and Amend J. P. (2015) Catabolic rates, population sizes and doubling/replacement times of microorganisms in natural settings. *Am. J. Sci.* **315**, 167–203.

LaRowe D. E. and Amend J. P. (2016) The energetics of anabolism in natural settings. *ISME J.* **10**, 1285–1295.

Lee R. W. and Childress J. J. (1994) Assimilation of inorganic nitrogen by marine invertebrates and their chemoautotrophic and methanotrophic symbionts. *Appl. Environ. Microbiol.* **60**, 1852–1858.

Malahoff A., Kolotyrkina I. Y., Midson B. P. and Massoth G. J. (2006) A decade of exploring a submarine intraplate volcano: hydrothermal manganese and iron at Lo'ihi volcano, Hawai'i. *Geochem. Geophys. Geosyst.* **7**, Q06002.

McCollom T. M. and Shock E. L. (1997) Geochemical constraints on chemolithoautotrophic metabolism by microorganisms in seafloor hydrothermal systems. *Geochim. Cosmochim. Acta* **61**, 4375–4391.

McCollom T. M. (2007) Geochemical constraints on sources of metabolic energy for chemolithoautotrophy in ultramafic-hosted deep-sea hydrothermal systems. *Astrobiology* **7**, 933–950.

McIlvin M. R. and Casciotti K. L. (2010) Fully automated system for stable isotopic analyses of dissolved nitrous oxide at natural abundance levels. *Limnol. Oceanogr.: Methods* **8**, 54–66.

Meador T. B., Aluwihare L. I. and Mahaffey C. (2007) Isotopic heterogeneity and cycling of organic nitrogen in the oligotrophic ocean. *Limnol. Oceanogr.* **52**, 934–947.

Mehta M. P., Butterfield D. A. and Baross J. A. (2003) Phylogenetic diversity of nitrogenase (nifH) genes in deep-sea and hydrothermal vent environments of the Juan de Fuca Ridge. *Appl. Environ. Microbiol.* **69**, 960–970.

Miroshnichenko M. L., Kostrikina N. A., Chernyh N. A., Pimenov N. V., Tourova T. P., Antipov A. N., Spring S., Stackebrandt E. and Bonch-Osmolovskaya E. A. (2003) *Caldithrix abyssi* gen. nov., sp nov., a nitrate-reducing, thermophilic, anaerobic bacterium isolated from a Mid-Atlantic Ridge hydrothermal vent, represents a novel bacterial lineage. *Int. J. Syst. Evol. Microbiol.* **53**, 323–329.

Moyer C. L., Dobbs F. C. and Karl D. M. (1994) Estimation of diversity and community structure through restriction length polymorphism distribution analysis of bacterial 16S ribosomal RNA genes from a microbial mat at an active hydrothermal system, Loihi Seamount, Hawaii. *Appl. Environ. Microbiol.* **60**, 871–879.

Moyer C. L., Dobbs F. C. and Karl D. M. (1995) Phylogenetic diversity of the bacterial community from a microbial mat at an active, hydrothermal vent system, Loihi Seamount, Hawaii. *Appl. Environ. Microbiol.* **61**, 1555–1562.

Moyer C. L., Tiedje J. M., Dobbs F. C. and Karl D. M. (1998) Diversity of deep-sea hydrothermal vent *Archaea* from Loihi Seamount, Hawaii. *Deep-Sea Res. Part II* **45**, 303–317.

Offre P., Spang A. and Schleper C. (2013) Archaea in biogeochemical cycles. *Annu. Rev. Microbiol.* **67**, 437–457.

Osburn M. R., LaRowe D. E., Momper L. M. and Amend J. P. (2014) Chemolithotrophy in the continental deep subsurface: Sanford Underground Research Facility (SURF), USA. *Front. Microbiol.* **5**, 610.

Ottley C. J., Davison W. and Edmunds W. M. (1997) Chemical catalysis of nitrate reduction by iron (II). *Geochim. Cosmochim. Acta* **61**, 1819–1828.

Pérez-Rodríguez I., Bohnert K. A., Cuebas M., Keddis R. and Vetriani C. (2013a) Detection and phylogenetic analysis of the membrane-bound nitrate reductase (Nar) in pure cultures and microbial communities from deep-sea hydrothermal vents. *FEMS Microbiol. Ecol.* **86**, 256–267.

Perez-Rodriguez I.M., Foustoukos D., Fogel M.L., Sievert S.M. (2013) Isotopic signatures associated with growth and metabolic activities of chemosynthetic nitrate-reducing microbes from deep-sea hydrothermal vents. Abstract B13C–0492 presented at 2013 Fall Meeting, AGU, San Francisco, Calif., 9–13 Dec.

Price R. E., LaRowe D. E., Italiano F., Savov I., Pichler T. and Amend J. P. (2015) Subsurface hydrothermal processes and the bioenergetics of chemolithoautotrophy at the shallow-sea vents off Panarea Island (Italy). *Chem. Geol.* **407–408**, 21–45.

Rassa A. C., McAllister S. M., Safran S. A. and Moyer C. L. (2009) *Zeta-Proteobacteria* dominate the colonization and formation of microbial mats in low-temperature hydrothermal vents at Loihi Seamount, Hawaii. *Geomicrobiol. J.* **26**, 623–638.

Santoro A. E. and Casciotti K. L. (2011) Enrichment and characterization of ammonia- oxidizing archaea from the open ocean: phylogeny, physiology and stable isotope fractionation. *ISME J.* **5**, 1796–1808.

Schloss P. D., Westcott S. L., Ryabin T., Hall J. R., Hartmann M., Hollister E. B., Lesniewski R. A., Oakley B. B., Parks D. H., Robinson C. J., Sahl J. W., Stres B., Thallinger G. G., Van Horn D. J. and Weber C. F. (2009) Introducing mothur: open-source, platform-independent, community-supported software for describing and comparing microbial communities. *Appl. Environ. Microbiol.* **75**, 7537–7541.

Schulte M. D., Shock E. L. and Wood R. H. (2001) The temperature dependence of the standard-state thermodynamic

properties of aqueous nonelectrolytes. *Geochim. Cosmochim. Acta* **65**, 3919–3930.

Scott J. J., Breier J. A., Luther, III, G. W. and Emerson D. (2014) Microbial iron mats at the Mid-Atlantic Ridge and evidence that Zetaproteobacteria may be restricted to iron-oxidizing marine systems. *PLoS One* **10**, e0119284-e0119284.

Sedwick P. N., McMurtry G. M. and MacDougall J. D. (1992) Chemistry of hydrothermal solutions from Pele's vents, Loihi Seamount, Hawaii. *Geochim. Cosmochim. Acta* **56**, 3643–3667.

Shock E. L. and Helgeson H. C. (1988) Calculation of the thermodynamic and transport properties of aqueous species at high pressures and temperatures: correlation algorithms for ionic species and equation of state predictions to 5 kb and 1000 C. *Geochim. Cosmochim. Acta* **52**, 2009–2036.

Shock E. L. and Helgeson H. C. (1990) Calculation of the thermodynamic and transport properties of aqueous species at high pressures and temperatures: standard partial molal properties of organic species. *Geochim. Cosmochim. Acta* **54**, 915–945.

Shock E. L., Helgeson H. C. and Sverjensky D. A. (1989) Calculation of the thermodynamic and transport properties of aqueous species at high pressures and temperatures: standard partial molal properties of inorganic neutral species. *Geochim. Cosmochim. Acta* **53**, 2157–2183.

Shock E. L., Oelkers E. H., Johnson J. W., Sverjensky D. A. and Helgeson H. C. (1992) Calculation of the thermodynamic properties of aqueous species at high pressures and temperatures. Effective electrostatic radii, dissociation constants and standard partial molal properties to 1000 C and 5 kbar. *J. Chem. Soc. Faraday Trans.* **88**, 803–826.

Shock E. L. and Holland M. E. (2004) Geochemical energy sources that support the subsurface biosphere. In *The Subseafloor Biosphere at Mid-ocean Ridges* (eds. W. S. D. Wilcock, E. F. Delong, D. S. Kelley, J. A. Baross and S. C. Cary). American Geophysical Union, Washington, D.C..

Sigman D. M., Casciotti K. L., Andreani M., Barford C., Galanter M. and Böhlke J. K. (2001) A bacterial method for the nitrogen isotopic analysis of nitrate in seawater and freshwater. *Anal. Chem.* **73**, 4145–4153.

Sigman D. M., Granger J., DiFiore P. J., Lehmann M. M., Ho R., Cane G. and van Geen A. (2005) Coupled nitrogen and oxygen isotope measurements of nitrate along the eastern North Pacific margin. *Global Biogeochem. Cycles* **19**, GB4022.

Sigman D. M., DiFiore P. J., Hain M. P., Deutsch C., Wang Y., Karl D. M., Knapp A. N., Lehmann M. F. and Pantoja S. (2009) The dual isotopes of deep nitrate as a constraint on the cycle and budget of oceanic fixed nitrogen. *Deep Sea Res. Part I* **56**, 1419–1439.

Smirnov A., Hausner D., Laffers R., Strongin D. R. and Schoonen M. A. A. (2008) Abiotic ammonium formation in the presence of Ni–Fe metals and alloys and its implications for the Hadean nitrogen cycle. *Geochem. Trans.* **9**.

Sogin M. L., Morrison H. G., Huber J. A., Mark Welch D., Huse S. M., Neal P. R., Arrieta J. M. and Herndl G. J. (2006) Microbial diversity in the deep sea and the underexplored "rare biosphere". *Proc. Natl. Acad. Sci. U.S.A.* **103**, 12115–12120.

Summers D. P. and Chang S. (1993) Prebiotic ammonia from reduction of nitrite by iron (II) on the early Earth. *Nature* **365**, 630–633.

Sverjensky D. A., Shock E. L. and Helgeson H. C. (1997) Prediction of the thermodynamic properties of aqueous metal complexes to 1000 C and 5 kb. *Geochim. Cosmochim. Acta* **61**, 1359–1412.

Swingley W. D., Meyer-Dombard D. R., Shock E. L., Alsop E. B., Falenski H. D., Havig J. R. and Raymond J. (2012) Coordinating environmental genomics and geochemistry reveals metabolic transitions in a hot spring ecosystem. *PLoS ONE* **7**, e38108.

Takai K., Moyer C. L., Miyazaki M., Nogi Y., Hirayama H., Nealson K. H., Horikoshi K. (2005) Marinobacter alkaliphilus sp nov., a novel alkaliphilic bacterium isolated from subseafloor alkaline serpentine mud from Ocean Drilling Program Site 1200 at South Chamorro Seamount, Mariana Forearc. Extremophiles: life under extreme conditions 9. pp. 17–27.

Tanger J. C. and Helgeson H. C. (1988) Calculation of the thermodynamic and transport properties of aqueous species at high pressures and temperatures; revised equations of state for the standard partial molal properties of ions and electrolytes. *Am. J. Sci.* **288**, 19–98.

Teske A., Callaghan A. V. and LaRowe D. E. (2014) Biosphere frontiers of subsurface life in the sedimented hydrothermal system of Guaymas Basin. *Front. Microbiol.* **5**, 362.

Vetriani C., Voordeckers J. W., Crespo-Medina M., O'Brien C. E., Giovannelli D. and Lutz R. A. (2014) Deep-sea hydrothermal vent Epsilonproteobacteria encode a conserved and widespread nitrate reduction pathway (Nap). *ISME J.* **8**, 1510–1521.

Von Damm K. L., Edmond J. M., Grant B., Measures C. I., Walden B. and Weiss R. F. (1985) Chemistry of submarine hydrothermal solutions at 21 N, East Pacific Rise. *Geochim. Cosmochim. Acta* **49**, 2197–2220.

Wang F. P., Zhou H. Y., Meng J., Peng X. T., Jiang L. J., Sun P., Zhang C. L., Van Nostrand J. D., Deng Y., He Z. L., Wu L. Y., Zhou J. H. and Xiao X. (2009) GeoChip-based analysis of metabolic diversity of microbial communities at the Juan de Fuca Ridge hydrothermal vent. *Proc. Natl. Acad. Sci. U.S.A.* **106**, 4840–4845.

Wankel S. D., Kendall C., Pennington J. T., Chavez F. P. and Paytan A. (2007) Nitrification in the euphotic zone as evidenced by nitrate dual isotopic composition: observations from Monterey Bay, California. *Global Biogeochem. Cycles* **21**, GB2009.

Wankel S. D., Buchwald C., Ziebis W., Wenk C. B. and Lehmann M. F. (2015) Nitrogen cycling in the deep sedimentary biosphere: nitrate isotopes in porewaters underlying the oligotrophic North Atlantic. *Biogeosciences* **12**, 7483–7502.

Wheat C. G., Jannasch H. W., Plant J. N., Moyer C. L., Sansone F. J. and McMurtry G. M. (2000) Continuous sampling of hydrothermal fluids from Loihi Seamount after the 1996 event. *J. Geophys. Res. Solid Earth* **105**, 19353–19367.

Winkel M., de Beer D., Lavik G., Peplies J. and Mußmann M. (2014) Close association of active nitrifiers with *Beggiatoa* mats covering deep-sea hydrothermal sediments. *Environ. Microbiol.* **16**, 1612–1626.

Xie X., Wang F., Guo L., Chen Z., Sievert S. M., Meng J., Huang G., Li Y., Yan Q., Wu S., Wang X., Chen S., He G., Xiao X. and Xu A. (2010) Comparative metagenomics of microbial communities inhabiting deep-sea hydrothermal vent chimneys with contrasting chemistries. *ISME J.* **5**, 414–426.

Associate editor: Jeffrey C. Alt